Mechanisms of infection and response of the fungal wheat pathogen *Zymoseptoria tritici* during compatible, incompatible and non-host interactions

Sandra V. Gomez-Gutierrez[1], Cassidy R. Million[2], Namrata Jaiswal[2], Michael Gribskov[3], Matthew Helm[2], and Stephen B. Goodwin[2#]

[1] Department of Botany and Plant Pathology, 915 Mitch Daniels Blvd., Purdue University, West Lafayette, IN 47907-2054

[2] Crop Production and Pest Control Research Unit, USDA–Agricultural Research Service, 915 Mitch Daniels Blvd. , West Lafayette, IN 47907-2054

[3] Department of Biological Sciences, 915 Mitch Daniels Blvd., Purdue University, West Lafayette, IN 47907-2054

[#]Corresponding Author: Steve.Goodwin@USDA.gov

Zymoseptoria tritici* incites Septoria tritici blotch, a disease causing significant annual yield losses in wheat. To investigate infection phase-specific gene expression in the pathogen we analyzed gene expression during infection of susceptible (Taichung 29) and resistant (Veranopolis and Israel 493) wheat cultivars, plus the non-host species barley at 1, 3, 6, 10, 17 and 23 days post-inoculation (DPI). There were dramatic differences in pathogen gene expression at 10 DPI in the compatible compared to both incompatible interactions. The largest differences in pathogen gene expression occurred at 3 DPI in both compatible and incompatible interactions compared to the non-host interaction. Thirty-one putative effectors had early expression in the compatible interaction. Subsequent subcellular localization studies using *Agrobacterium*-mediated transient expression in *Nicotiana

***benthamiana* revealed that most candidate effectors localized to the nucleus and cytosol, and two localized to mobile cytosolic bodies, suggesting involvement in intracellular signaling or host gene regulation. Mycgr3109710, which localized to cytosolic bodies, belongs to the non-plant PR-1-like protein family implicated in virulence in other pathogens. Comparison of pathogen gene expression in resistant and susceptible hosts, in which an initial colonization is established, versus in the non-host species, allowed us to identify genes involved in establishing infection. Comparison of the compatible and incompatible interactions identified pathogen genes involved in transition from biotrophic to necrotrophic growth at 10 DPI. In addition, we contribute to the understanding of candidate effectors that are activated early during infection and might be involved in the initial plant immunity suppression.**

Key words: *Zymoseptoria tritici*, wheat, fungal pathogen, effectors, localization,

Introduction

Zymoseptoria tritici is a fungal pathogen in the class Dothideomycetes that causes Septoria tritici blotch (STB) disease of bread wheat (*Triticum aestivum* L.) and durum wheat (*T. durum*) (Kettles & Kanyuka, 2016; Palma-Guerrero et al., 2017). STB is one of the most yield-limiting diseases of wheat globally and may result in fifty percent yield loss, especially in regions with high humidity and mild temperatures (Mekonnen et al., 2020; N. Yang et al., 2022). *Z. tritici* is a hemibiotroph that transitions to necrotrophic growth after a prolonged 7-to-10-day latent period (Ponomarenko et al., 2011; Rudd et al., 2015). During the biotrophic growth phase, the pathogen circumvents recognition through suppression of host immune responses, likely by

translocating virulence (effector) proteins. During the necrotrophic phase, the fungus degrades host tissue and presumably extracts nutrients from host plant cells (Marshall et al., 2011; Steinberg, 2015). The hemibiotrophic lifestyle of *Z. tritici* coupled with the availability of a complete, chromosome-level genome makes this fungal pathogen an attractive model to investigate infection phase-specific gene expression (Goodwin et al., 2011).

Though *Z. tritici* is a hemibiotroph, our knowledge of its infection strategy and lifestyle transition remains limited. Nevertheless, comprehensive RNA sequencing analyses have provided insights into host and pathogen gene expression during a compatible interaction (Rudd et al., 2015; Yang et al., 2013), transcriptome signatures associated with blastospore and mycelial growth (Francisco et al., 2019), as well as differences in gene expression among *Z. tritici* strains (Palma-Guerrero et al., 2017). Studies have also assessed plant gene expression in resistant-host (incompatible) and non-host interactions (Orton et al., 2017; Reilly et al., 2021), and one study compared the pathogen gene expression profile during infection in a compatible host (*T. aestivum* L.) and a non-host (*Brachypodium distachyon*) (Kellner et al., 2014). Kellner et al. (2014) found that many wheat-specific, up-regulated genes in *Z. tritici* encode proteins with putative secretion signals that may have a functional role in host invasion. The most highly differentially expressed genes (DEG) in *Z. tritici* during the comparison between the compatible and the non-host interaction showed signatures of positive selection, and can be considered as candidates for potential roles in host specialization of this pathogen (Kellner et al., 2014).

Differential responses of pathogens to susceptible, resistant, and non-host species are often determined by the molecular mechanisms underlying the interactions as well as virulence (effector) proteins (Selin et al., 2016). Pathogens often secrete effectors, in part, to circumvent host innate immune responses (Petit-Houdenot & Fudal, 2017; Selin et al., 2016). Once

translocated to the host apoplast or cytosol, effector proteins interfere with cell surface-mediated and intracellular-mediated immune responses, thereby promoting pathogenesis and disease development. Although *Z. tritici* is considered one of the most economically important diseases of wheat, few effector proteins have been functionally characterized (Motteram et al., 2009; Marshall et al., 2011; Mirzadi Gohari et al., 2015; Rudd et al., 2015; Ben et al., 2015; Karki et al., 2021). For example, the *Z. tritici* Mg3LysM effector is expressed during early onset of disease development and suppresses chitin-induced defense responses in wheat (Marshall et al., 2011; Rudd et al., 2015). Furthermore, Karki et al. (2021) recently identified an effector from *Z. tritici*, ZtSSP2, that is expressed at 2 days post-inoculation (DPI) and interacts with a wheat E3 ubiquitin ligase (TaE3UBQ). Intriguingly, virus-induced gene silencing of TaE3UBQ resulted in increased *Z. tritici* susceptibility, suggesting TaE3UBQ may function as a regulator of wheat defense responses, and that ZtSSP2 may suppress TaE3UBQ ligase activity to promote *Z. tritici* pathogenicity (Karki et al., 2021).

In wheat, there have been twenty-two reported resistance genes (R-genes) to *Z. tritici* (Saintenac et al., 2021). *Stb6* encodes a conserved wall-associated kinase (WAK) with an extracellular domain that recognizes the apoplastic AvrStb6 effector from *Z. tritici* (Brown et al., 2015; Saintenac et al., 2018; Zhong et al., 2017). The resistance protein *Stb16q* also encodes a cysteine-rich wall-associated-like receptor kinase that presumably recognizes a fungal carbohydrate to trigger a resistance response (Saintenac et al., 2021). Intriguingly, *Stb16q* confers full broad-spectrum resistance against 64 geographically diverse isolates of *Z. tritici* (Saintenac et al., 2021). Moreover, the *Stb9* resistance protein recognizes AvrStb9, a secreted protease-like protein with a predicted S41 conserved domain and triggers an immune response following the gene-for-gene model (Amezrou et al., 2023). However, the function of *Stb9* is still

not clear as it might be acting as a classical receptor protein, an inhibitor of AvrStb9 protease activity, or as the guard protein of the AvrStb9 target protein (Amezrou et al., 2023).

Non-host resistance (NHR) is also commonly broad spectrum and, hence, likely more durable (Ayliffe & Sørensen, 2019; Gill et al., 2015). Several types of NHR involve a hypersensitive response as it occurs in qualitative resistance conferred by Avr recognition (Panstruga & Moscou, 2020). Evidence that Avr recognition is involved in NHR was found by studying the closest homologues of the *Z. tritici* Avr3D1 in sister fungal species that are nonpathogenic in wheat. The homologous genes induce a strong defense response in wheat when expressed in a virulent mutant strain of *Z. tritici*, suggesting they contribute to establishing host range and are involved in NHR (Meile et al., 2022). Barley (*Hordeum vulgare* subsp. *vulgare*) is closely related to wheat and is an important cereal crop that is infected by *Z. passerinii*, a species that is closely related to *Z. tritici.* Barley is a non-host of *Z. tritici* and thus shows strong resistance to this pathogen. Identifying and comparing DEGs in *Z. tritici* during a non-host interaction with barley is central to testing whether similar virulence factors and molecular pathways are expressed during compatible, incompatible (R-gene) and non-host interactions. In addition, studying pathogen gene expression during a non-host interaction with a closely related grass species of wheat can identify candidate effectors that determine host specificity, and, in the future, possible host target proteins. This information can be transferred from barley into the *Z. tritici* – wheat pathosystem to provide additional sources for breeding resistance in wheat.

In the present study, we investigate pathogen gene responses during interactions with susceptible, resistant, and non-host cultivars, using a time course of transcriptomic data covering distinct phases of the infection process. We examine three types of interaction, compatible interaction with a susceptible wheat cultivar, two incompatible interactions with resistant wheat

cultivars Veranopolis and Israel 493, and a non-host interaction with barley, to test the hypothesis that different genes are involved in each interaction. We identify thirty-one putative effectors that are expressed during early disease development in a compatible interaction and we investigated their subcellular localizations using *Agrobacterium*-mediated transient expression in *Nicotiana benthamiana*.

Results

Differential gene expression patterns between compatible, R-gene and non-host interactions.

Differential gene expression in *Z. tritici* was determined between three types of plant-pathogen interactions: (1) a compatible interaction with the highly susceptible wheat cultivar Taichung 29; (2) two incompatible interactions with resistant wheat cultivars Veranopolis, which carries the *Stb2* and *Stb6* resistance gene, and Israel 493, which carries the *Stb3* and *Stb6* resistance genes; and (3) a non-host interaction with the barley cultivar Kindred (Table 1). Comparison of pathogen gene expression in the susceptible and resistant hosts, in both of which an initial infection is established, versus the non-host species, in which reduced pathogen growth is seen, allows us to identify genes involved in establishing infection. Comparison of pathogen gene expression in the susceptible and resistant cultivars identifies genes that are necessary for the transition from biotrophic to necrotrophic growth. We measured the gene expression at six time points: 1, 3, 6, 10, 17 and 23 days post inoculation (DPI).

Gene expression analysis during the interaction of *Z. tritici* and its wheat host.

Gene expression patterns in the replicates of the compatible and the two incompatible interactions were explored with principal component analysis (PCA) (Fig. 1). PCA shows that

gene expression is very similar in the compatible and incompatible interactions early in infection (1, 3 DPI) (Fig. 1.). Most replicate samples are well clustered, indicating limited biological variation within replicate time points. At 6 DPI, gene expression in the compatible and incompatible interactions begins to diverge. And at 10 DPI, the compatible interaction is distinctly separated from the incompatible interactions, primarily along principal component 2, while gene expression in the incompatible samples at 10 DPI remains relatively similar to that of 6 DPI. A similar pattern is observed at 17 and 23 DPI (Fig. 2), where the compatible interaction forms a separate cluster from the incompatible interaction. The 17 and 23 DPI points cluster together for both compatible and incompatible interaction, suggesting little change in gene expression from 17 to 23 DPI. The replicate points for the incompatible interactions show considerable variability due to the reduced read counts obtained at the late infection in the incompatible interactions, but the trend is clear. The highest number of DEGs in *Z. tritici* was observed at 10 DPI when comparing the compatible interaction on the susceptible cultivar Taichung 29 with both incompatible interactions on the *Stb2*-carrying cultivar Veranopolis (601 DEGs) and on the *Stb3*-carrying cultivar Israel 493 (587 DEGs) (Table 2). A total of 275 and 226 genes in *Z. tritici* were found to be up-regulated at 10 DPI during the compatible interaction compared to the incompatible *Stb2* and the *Stb3* interactions, respectively. This rapid and sudden activation of a large number of DEGs in *Z. tritici* at 10 DPI in the compatible interaction corresponds with the lifestyle transition from the biotrophic to necrotrophic stage. Of these, 183 up-regulated and 234 down-regulated genes were common between the comparisons of the compatible interaction against the two incompatible interactions (Fig. 3). This indicates that many *Z. tritici* genes (183 or 58%) are expressed only during the compatible interaction but not

during any of the incompatible interactions, and that many genes (234 or 52%) are expressed in the pathogen exclusively during both incompatible interactions.

We determined the DEGs in *Z. tritici* during the incompatible interaction with Veranopolis compared to the incompatible interaction with Israel 493. Only 1 DEG was up-regulated in *Z. tritici* inoculated on the Veranopolis cultivar compared to Israel 493 at 6 DPI. In total 12, 14 and 3 genes were found to be differentially expressed at 10, 17 and 23 DPI (Table 2), respectively. No DEGs were identified when comparing the two incompatible interactions at 1 and 3 DPI. This shows that *Z. tritici* follows a nearly identical pattern of gene expression during its interaction with both resistant wheat cultivars.

The unique and common genes between time points in the compatible interaction compared to the incompatible interaction with cultivar Veranopolis were identified. In total, 249 up-regulated DEGs were unique at 10 DPI, 17 up-regulated DEGs were unique at 23 DPI and 4 unique DEGs were up-regulated at 17 DPI (Fig. 4). These results demonstrate that the number of DEGs that is exclusively activated in *Z. tritici* at 10 DPI is remarkably high compared to other time points, which indicates that a defined shift in gene expression occurs at this stage, and that many of these genes might have a role in the transition to the necrotrophic phase and the consequent tissue degradation and nutrient extraction processes. The same pattern of differential gene expression was observed at 10, 17 and 23 DPI in the comparison of *Z. tritici* grown on the susceptible cultivar Taichung 29 compared to the resistant cultivar Israel 493 (Fig. 5).

Gene Ontology and enrichment analysis during host interactions.

Zymoseptoria tritici DEGs were grouped according to their putative roles in biological processes (BP), molecular functions (MF) and cellular components (CC) as established by the

Gene Ontology Consortium (http://www.geneontology.org/). The up-regulated genes in *Z. tritici* at 10 DPI in the compatible interaction are significantly enriched in the GO categories involved in synthesis of new compounds, including: organonitrogen compound metabolic process (GO:1901564), macromolecule metabolic process (GO:0043170) and macromolecule biosynthetic process (GO:0009059), ribonucleoprotein complex biogenesis (GO:0022613), pyrimidine-containing compound biosynthetic process (GO:0072528), nitrogen compound biosynthetic process (GO:0044271), and amide biosynthetic process (GO:0043604). Numerous GO terms related to ribosome components are enriched including small ribosomal subunit (GO:0015935), cytosolic small ribosomal subunit (GO:0022627), and structural constituent of ribosome (GO:0003735). Additional GO terms enriched were in the categories nucleic acid binding (GO:0003676) and rRNA binding (GO:0019843). At 17 DPI the enriched GO categories in the up-regulated genes are transmembrane transporter activity (GO:0022857), passive transmembrane transporter activity (GO:0022803), monoatomic ion channel activity (GO:0005216), and monoatomic ion transmembrane transport (GO:0034220). Some GO terms were significantly enriched in the down-regulated genes at 23 DPI in the compatible interaction compared to the R-gene interactions. These included hydrolase activity acting on acid anhydrides (GO:0016817), guanyl ribonucleotide binding (GO:0032561) and GTPase activity (GO:0003924) (Supplementary Fig. S1).

The KEGG pathway enrichment analysis showed that 13 pathways were significantly enriched in the up-regulated genes at 10 DPI during the compatible interaction compared to both incompatible interactions. The top five enriched pathways were carbon metabolism, biosynthesis of antibiotics, biosynthesis of secondary metabolites, glycolysis and gluconeogenesis. In contrast, at 23 DPI only 3 pathways were enriched in the up-regulated genes in the compatible

interaction compared to the incompatible interaction including carbon metabolism, biosynthesis of antibiotics, and glycolysis and gluconeogenesis.

In the compatible interaction compared to the incompatible interactions, we observed a significant up-regulation of genes at 10 days post-infection (DPI) that encode carbohydrate-active enzymes (CAZymes). Among these, we identified eight glycoside hydrolases (GHs) and one carbohydrate esterase (CE), all of which are cell wall-degrading enzymes (CWDEs). This finding supports the proposed role of these up-regulated genes at 10 DPI in tissue degradation and nutrient extraction, processes crucial for sustaining the necrotrophic stage. Additionally, our analysis revealed 10 glycosyltransferases (GTs) and 10 enzymes with auxiliary activity (AA) among the up-regulated genes (Supplementary Fig. S3). Families of AA enzymes involved in oxidation of aromatic compounds and fungal growth such as the multicopper oxidase family (AA1), and the alcohol oxidase subfamily (AA3_3) were up-regulated in both comparisons between the compatible interaction and the two incompatible interactions.

In contrast, among the down-regulated genes at 10 DPI, we annotated 12 genes as GHs, 8 as GTs, and 11 enzymes in the AA category. Families of AA enzymes involved in detoxification, oxidation of compounds, and fungal growth such as the benzoquinone reductase family (AA6), the alcohol dehydrogenase subfamily (AA3_2) and the alcohol oxidase subfamily (AA3_3) were down-regulated in the comparisons. This observation shows the activation of CAZymes in *Z. tritici* at 10 DPI in the incompatible interactions compared to the compatible interaction. It indicates that the fungus is deploying a set of molecular compounds at the transition stage during an incompatible interaction, possibly to counteract the resistant response from the wheat cultivars.

We also identified predicted small, secreted proteins (SSPs) in the set of DEGs. Notably, at 10 DPI, 26 SSPs were down-regulated compared to 14 and 13 SSPs that were up-regulated in the compatible interaction compared to the *Stb2*- and *Stb3*-gene interactions, respectively.

Gene expression analysis during a non-host interaction.

In contrast to the comparison between the compatible interaction and the incompatible interactions, the largest differences between the compatible and the non-host interaction are seen at 3 DPI. There were 171 DEGs in *Z. tritici*, of which 124 were up-regulated and 47 were down-regulated (Table 3) in comparison to the non-host interaction with *H. vulgare*. These genes that are up-regulated in the compatible interaction can potentially have a role in the ability of the pathogen to establish the initial infection in the susceptible host. There were 154 DEGs when comparing the incompatible interaction between *Z. tritici* and the Veranopolis (*Stb2*) resistant cultivar with the non-host interaction (Table 3). This is similar to the 160 DEGs in *Z. tritici* in the incompatible interaction between *Z. tritici* and the Israel 493 (*Stb3*) resistant cultivar compared to the non-host interaction (Table 3). At 3 DPI, there were 98 (75%) up-regulated and 40 (67%) down-regulated *Z. tritici* genes that were common in both compatible and incompatible interactions on wheat compared to the non-host interaction on barley (Fig. 6). This reveals that at 3 DPI *Z. tritici* activates a large number of genes presumably involved in mechanisms of host recognition that are the same in both the compatible and incomaptible interactions.

The numbers of up-regulated DEGs at 10 DPI show a slight increase in contrast to the previous time point at 6 DPI when comparing both the compatible and incompatible interactions against the non-host interaction. At 17 and 23 DPI, for the genes for which we were able to retrieve measurable counts, we observed higher numbers of DEGs in the compatible interaction

than the numbers of DEGs at 17 and 23 DPI in the incompatible interactions compared to the non-host interaction. This suggests that from 17 to 23 DPI the fungal responses during both incompatible and non-host interactions follow a similar pattern of gene activation and that *Z. tritici* probably activates comparable mechanisms to interact with both resistant and non-host species. The fact that we were not able to retrieve counts for most of the genes predicted in the *Z. tritici* genome at 17 and 23 DPI in both incompatible and non-host interactions also reveals that there is a significant reduction in the fungal biomass compared to 1 to 10 DPI in these interactions and compared to the compatible interaction.

To find unique up-regulated DEGs that are activated at certain time points during the compatible and incompatible interactions compared to the non-host interaction and differentiate them from those that were expressed steadily, we determined unique and shared up-regulated DEGs between the sampling days. In the compatible interaction compared to the non-host interaction, there were 52 up-regulated DEGs that were unique at 3 DPI, followed by 50 up-regulated DEGs shared at 1 and 3 DPI (Fig. 7) when comparing the compatible interaction with the non-host interaction between *Z. tritici* and barley. There were 45 unique DEGs in *Z. tritici* at 3 DPI, followed by 45 DEGs at both 1 and 3 DPI when comparing the incompatible interaction on Veranopolis (*Stb2*) with the non-host interaction (Fig. 8). The combined number of up-regulated DEGs at 1 and 3 DPI is much higher than the unique genes at other time points, which indicates that the main difference in the pattern of gene activation between the incompatible interaction and the non-host interaction occurs at the beginning of the infection process.

We also wanted to determine the unique and shared up-regulated DEGs at different sampling days during the incompatible interaction on Israel 493 (*Stb3*) versus the non-host interaction on barley. In total, 46 up-regulated DEGs were observed at 3 DPI, followed by 43

upregulated DEGs shared at 1 and 3 DPI (Figure 9). Taken together, 89 DEGs are being up-regulated during the early stage of infection, which represents more than those DEGs at 10 DPI. This supports the idea of an early recognition of the host species from 1 to 3 DPI in the incompatible interactions, and the subsequent activation of a large number of genes at 3 DPI. Presumably, the fungus recognizes and is able to penetrate the leaves of both the susceptible and resistant host species during the first three days after inoculation by activating a large number of genes that are not expressed during a non-host interaction.

Gene Ontology and enrichment analyses during the non-host interaction on barley.

The significantly enriched GO categories in the up-regulated genes at 3 DPI in the compatible interaction included those involved in light responses in *Z. tritici* including phototransduction (GO:0007602), detection of abiotic stimulus (GO:0009582), detection of external stimulus (GO:0009581), detection of light stimulus (GO:0009583), and photoreceptor activity (GO:0009881) (Fig. 12). Also at 1 DPI, the enriched GO categories were involved in detoxification processes including oxidoreductase activity (GO:0016491) and succinate dehydrogenase activity (GO:0000104). At 6 DPI the enriched GO categories are involved in reinforcement of the cell wall including external encapsulating structure (GO:0030312), cell wall (GO:0005618), cell periphery, and structural constituent of cell wall (GO:0005199).

The down-regulated genes in *Z. tritici* at 10 DPI in the comparison between the compatible interaction and the non-host interaction were significantly enriched in the GO categories involved in autophagy including vacuolar acidification (GO:0007035), intracellular pH reduction (GO:0051452), regulation of intracellular pH (GO:0051453), vacuolar proton

transporting (GO:0000221), ubiquitin ligase complex (GO:0019005) and nuclear ubiquitin ligase complex (GO:0043224).

The KEGG pathway enrichment analysis showed that 5 pathways were significantly enriched among the up-regulated genes at 1 DPI during the compatible interaction compared to the non-host interaction. These were glycolysis/gluconeogenesis, carbon metabolism, biosynthesis of secondary metabolites, biosynthesis of antibiotics and fructose and mannose metabolism. At 3 DPI three pathways were enriched which include pyruvate metabolism, carbon metabolism and glycolysis and gluconeogenesis.

Three glycoside hydrolases (GHs) were significantly up-regulated at 1 DPI, and 6 CAZymes were up-regulated at 3 DPI, including 1 glycosyl transferase (GT), 4 GHs and 1 carbohydrate-binding molecule (CBM). At 6 and 10 DPI, 3 GHs, 5 GTs and 1 CBM were up-regulated (Supplementary figure S4). Also at 1 and 3 DPI, we were able to detect 7 and 9 SSPs that were up-regulated in the compatible versus the non-host interaction.

Expression of *Z. tritici* candidate effectors during early disease development.

To gain further insight into *Z. tritici* pathogenicity, we leveraged a recently developed effector prediction pipeline and the predicted *Z. tritici* secretome to select thirty-one candidate effectors, using enhanced transcript abundance during the early stages of infection (1 and 3 DPI) as the primary criterion for selection. Specifically, we selected proteins that fulfilled the following selection criteria: (i) enriched transcript expression during early disease development; (ii) presence of a predicted signal peptide sequence; and (iii) absence of a predicted transmembrane domain. We next leveraged EffectorP (v.3.0) (Sperschneider & Dodds, 2022) to further refine our list of effector candidates. The selected effector candidates ranged in size from

68 to 554 amino acids (Table 4). Though the majority of the putative effectors do not contain subcellular-targeting peptide sequences, several encode predicted nuclear localization signals (NLS), chloroplast transit peptides (cTPs), or mitochondrial-targeting sequences (Table 4). One putative effector, Mycgr394290, includes multiple predicted subcellular localization signals including a cTP, mitochondrial targeting sequence, and a NLS (Table 4). Further examination of the candidate effectors revealed that two proteins, Mycgr3101991 and Mycgr3102792, contain predicted NLS, and one, Mycgr3106456, encoded a predicted cTP. Though most of the candidate effectors are annotated as uncharacterized, two candidate effectors are annotated as having peptidoglycan-binding LysM domains and are up-regulated at 1 and 3 DPI during the compatible interaction. Furthermore, two effector candidates encode Hce2-like domains; another effector candidate is annotated as an allergen V5/Tpx-1-related protein, another one as a heat shock protein, and one as a cerato-platanin protein.

Some of the effector candidates with reported annotation have been predicted to function as effectors or toxic compounds in other fungal plant pathogens, and some have been differentially expressed in previous transcriptome studies on *Z. tritici* (Mirzadi Gohari et al., 2015; Rudd et al., 2015; Yang et al., 2013). For example, five Hce2 domain-containing effectors have been identified in *Valsa mali*, the causal agent of apple Valsa canker. One of these effectors induced cell death when transiently expressed in *N. benthamiana* (Zhang et al., 2019). In the genome of the wheat pathogen *Fusarium graminearum*, there are two genes that putatively encode cerato-platanin proteins, which function as elicitors of defense responses on *Arabidopsis* leaves (Quarantin et al., 2019). A novel cerato-platanin-like effector protein from *Fusarium oxysporum f.* sp *cubense* triggers a hypersensitive response and systemic acquired resistance in tobacco (Li et al., 2019). Additionally, a *Sclerotinia sclerotiorum* cerato-platanin induces cell-

death in *N. benthamiana* and interacts with a PR-1 protein in the apoplast to facilitate infection (Yang et al., 2018). In addition, *Z. tritici* and *C. fulvum* LysM domain-containing effectors have previously been predicted and their functional roles have been characterized (Sánchez-Vallet et al., 2013; Tian et al., 2021). Overall, the evidence found in other fungal pathogens suggests that the candidate effectors identified in the present study might have a functional role at the early stages of infection.

We next analyzed the gene expression profiles of the thirty-one selected effector candidates across all the time points using the log-transformed normalized counts of each gene in the individual samples of the compatible interaction. Our analyses revealed three clusters of candidate effector genes based on the similarities of their gene expression patterns (Fig. 10). Each cluster contains candidate effector genes that are commonly regulated at specific time points. We found a cluster consisting of 10 candidate effectors which were commonly up-regulated at 1 and 3 DPI compared to the average relative expression of the 31 candidate effector genes selected. A second cluster contained 10 genes that were commonly up-regulated was identified at 10 and 17 DPI, and a third cluster of 11 genes with similar expression patterns was identified at 23 DPI (Fig. 10).

Subcellular localization patterns of *Z. tritici* effector-fluorescent protein fusions.

Having shown that several candidate effector proteins encode subcellular-targeting peptide sequences, we next investigated whether any of these putative effectors localized to specific plant cell compartments. To do this, we fused super Yellow Fluorescent Protein (sYFP) to the C-terminus of each mature (i.e., without the predicted signal peptide) candidate effector and transiently expressed them in *Nicotiana benthamiana* using *Agrobacterium*-mediated

transformation (agroinfiltration) and assessed their subcellular localization patterns using laser-scanning confocal microscopy (Helm et al., 2022; Jaiswal et al., 2023). Among the thirty-one selected candidate effectors, twenty-seven were successfully transformed into *Agrobacterium tumefaciens.* Hence, the remaining experiments focused on these twenty-seven putative effectors. Live-cell imaging of *N. benthamiana* epidermal cells revealed that fluorescence signals from twenty-one of the twenty-seven sYFP-tagged candidate effectors were indistinguishable from that of the free sYFP control and were thus considered to have a non-informative localization (Fig. 11). The fluorescence signal from four sYFP-tagged effector candidates, Mycgr3107904:sYFP, Mycgr346866:sYFP, Mycgr3104009:sYFP, and Mycgr3102849:sYFP, was predominantly localized within the cytosol with weak fluorescence observed in the nucleus (Fig. 12).

Intriguingly, Mycgr3109710:sYFP and Mycgr394290:sYFP labeled mobile cytosolic bodies (Fig. 13). We next performed immunoblot analyses to confirm the expression and integrity of the *Z. tritici* effector-fluorescent protein fusions in *N. benthamiana*. This assay revealed that of the twenty-seven candidate effectors screened, twenty-six accumulated at detectable levels when transiently expressed in *N. benthamiana.* One putative effector (Mycgr3106456) repeatedly failed to express detectable proteins, and another candidate effector (Mycgr3105182) accumulated protein at a lower molecular weight than predicted. For some putative effectors we consistently observed two protein bands, suggesting these proteins may undergo posttranslational modifications (Supplementary figure S5).

Discussion

Comparative RNAseq analysis clearly shows that different suites of genes are expressed by *Z. tritici* during biotrophic and necrotrophic infection stages. The comparison of the infection time course in the susceptible (compatible) host, and the two resistant (incompatible) hosts, allows us to identify genes that are necessary for or participate in the transition from biotrophic to necrotrophic growth stages. The sudden increase in the number of differentially expressed genes at 10 days post-inoculation was expected as previous studies have shown transcriptome reprogramming in *Z. tritici* during the transition to necrotrophy (Kellner et al., 2014; Palma-Guerrero et al., 2017; Rudd et al., 2015; F. Yang et al., 2013). Our results provide the first confirmation that the main difference in the pathogen gene expression in a compatible compared to an incompatible host interaction occurs at the transition stage rather than during the early infection stage (1-6 DPI). These results also reveal that *Z. tritici* deploys a similar gene activation pattern and comparable molecular mechanisms during the symptomless early stage of the disease in a compatible interaction compared to an incompatible host interaction.

In previous comparisons of host interactions vs a non-host interaction, investigators found that when other grass species, such as *Brachypodium distachyon* or *Agropyron repens*, are inoculated with *Z. tritici*, the pathogen can penetrate the leaf surface through stomata, but the infection is halted in the substomatal cavity (Kellner et al., 2014). This suggests an early recognition and interaction between the host and pathogen, during which *Z. tritici* can manipulate host defenses in susceptible wheat lines to colonize the plant and initiate the symptomless phase (Kellner et al., 2014).

Comparison of gene expression in susceptible and resistant wheat cultivars to gene expression in a non-host allows us to examine genes involved in initiating/supporting infection during the biotrophic phase. This is because, in both susceptible and resistant hosts, *Z. tritici* is

able to initiate a stomatal infection, while in the non-host it does not. This study provides the first confirmation that the transcriptomic response in *Z. tritici* is significantly different at the early infection stage in both compatible and incompatible interactions on resistant hosts compared to a non-host interaction with barley. Our results reveal that *Z. tritici* activates a different gene expression program and uses different molecular mechanisms at 1 and 3 DPI when interacting with susceptible or resistant wheat cultivars, compared to its program when interacting with a non-host species. This suggests that there is an early recognition mechanism in the pathogen that distinguishes between the host and a non-host species. It may be possible to manipulate this mechanism to develop broadly resistant wheat varieties.

The highest number of DEGs in *Z. tritici* when comparing the compatible interaction on the highly susceptible cultivar Taichung 29 with both incompatible interactions on resistant wheat cultivars was observed at 10 DPI. Interestingly, in a previous study, Yang et al. (2013) observed the highest number of differentially expressed *Z. tritici* transcripts in the necrotrophic stage (13 DPI) compared to 4 and 10 DPI in a compatible interaction with the susceptible wheat cultivar Sevin. In our study, we demonstrate that the main difference in the transcriptome reprogramming response in the pathogen in a compatible compared to an incompatible interaction occurs at the transition stage (10 DPI) rather than at the necrotrophic phase (13 DPI), revealing different molecular mechanisms in *Z. tritici* that are exclusively activated at 10 DPI and are determining the outcome of the infection in each type of interaction. On the other hand, Rudd et al. (2015) found that in a compatible interaction compared to growth in Czapek-Dox broth culture medium, the highest number of up-regulated genes in *Z. tritici* was observed at the transition to the necrotrophic stage (9 DPI), while in our study, it occurred at 10 DPI. Rudd et al. (2015) identified 1,389 DEGs at 9 DPI, while we found 601 and 587 total DEGs in the

compatible interaction compared to the *Stb2*-gene and *Stb3*-gene interactions, respectively. These findings indicate that significant transcriptional reprogramming in *Z. tritici* occurs during the transition stage, around 9-13 dpi, in a compatible interaction compared to fungal growth in culture media or to infection of a resistant host.

The analysis conducted by Yang et al. (2013) demonstrated distinct transcriptional responses during different phases of the infection. Their principal component analysis (PCA) showed separation between the 4-day, 10-day, and 13-day infected samples, representing the symptomless phase, the intermediate transition stage, and the necrotrophic phase, respectively. In our analyses, PCA identified four clusters for the replicates of the compatible interaction (C1: 1 and 3 DPI, C2: 6 DPI, C3: 10 DPI, C4: 17 and 23 DPI) (Figure 1). C1 contains all the replicates from both compatible and incompatible host interactions, revealing a similar gene activation in the fungus at 1 and 3 DPI. From 6 DPI, we observe the beginning of a different transcriptional response in the compatible and incompatible host interactions. This time point marks the separation of replicates from the compatible interaction into their own cluster. C3 and C4 are clearly separated from the replicates of the incompatible host interactions (Figures 1 and 2). This finding strongly suggests the existence of defining molecular processes in the pathogen that govern or result from the successful switch from the biotrophic phase to necrotrophic stage at 10 DPI, ultimately determining whether the interaction is compatible or incompatible. In our study, 1,504 genes at 1, 3, 6, and 10 DPI and 222 genes at 17 and 23 DPI were detectable and passed the normalization and filtering criteria for the comparison of the compatible and incompatible interactions. It is worth noting that the DEGs identified at 10 DPI account for approximately 40% of the normalized read counts, which highlights that a substantial proportion of fungal genes are being expressed during the transition to the necrotrophic stage in the compatible

interaction. Consequently, the identified DEGs reveal a very substantial transcriptome reprograming in the pathogen at 10 DPI to interact with a susceptible host compared to a resistant host. These genes are likely to be involved in molecular pathways that determine the ability of the pathogen to overcome the plant response and induce necrotic symptoms around 10 DPI in a compatible interaction. Interestingly, changes in gene expression of the pathogen are mirrored by those in the host, which corresponded to early and late points in the infection process (Adhikari et al., 2007). The host responded during early detection of the pathogen and then again when the pathogen transitioned from biotrophic to necrotrophic growth.

KEGG analysis identified biosynthesis of antibiotics and biosynthesis of secondary metabolites as significantly enriched pathways in the compatible interaction compared with both incompatible interactions at 10 DPI. Similarly, in a study conducted on *Bipolaris maydis* on resistant and susceptible non-CMS (cytoplasmic male sterility) maize genotypes, these same biosynthetic pathways were enriched exclusively for the interaction with the susceptible backgrounds during infection (Meshram et al., 2022). The authors concluded that the successful pathogenicity of *B. maydis* depends on pathogen fitness genes such as toxin-related effector molecules, cell wall degradation of the host, detoxification, and host defense evasion (Meshram et al., 2022). These findings agree with our observation that *Z. tritici* activated an arsenal of biosynthetic pathways, CAZymes including CWDEs, and SSPs during the transition to the necrotrophic stage in the compatible interaction. However, among the down-regulated genes, although we were not able to find significantly enriched pathways due to the low number of genes that were annotated, we found CAZymes and SSPs that were down-regulated at 10 DPI, such as the alcohol dehydrogenase CAZyme family (AA3_2). This group includes enzymes with important roles in the fungal life cycle and colonization of the host (Gutiérrez-Corona et al.,

2023). In *B. cinerea*, an alcohol dehydrogenase regulates fungal development, environmental adaptation and pathogenicity as observed in the morphology and virulence of knock-out mutants (DafaAlla et al., 2022). The benzoquinone reductase family (AA6) also was down-regulated, which contains intracellular enzymes involved in the biodegradation of aromatic compounds and in the protection of fungal cells from reactive quinone compounds (Levasseur et al., 2013). These findings indicate the activation of pathogen fitness genes and detoxification compounds in *Z. tritici* during interaction with the resistant cultivars at 10 DPI.

In the comparison between the compatible and the incompatible interactions against the non-host interaction with barley, the main difference in the *Z. tritici* transcriptional responses occurred at 1 and 3 DPI in all the comparisons evaluated. We identified 285, 261 and 269 DEGs at 1 and 3 DPI in the comparisons of the compatible, the *Stb2*-gene, and the *Stb3*-gene interactions with the non-host interaction, respectively. At 3 DPI the numbers of DEGs were always higher than the DEGs at 10 DPI for the three comparisons, which reveals that the main difference in the pattern of gene expression in the fungus during a host interaction compared to a non-host interaction occurs at the early stage of infection rather than during the transition stage. We detected 352 genes with measurable counts at 10 DPI, which reveals that the pathogen is able to grow and colonize to some extent in the non-host species. In a previous report (Kellner et al., 2014), the patterns of transcription in *Z. tritici* during infection in the susceptible wheat cultivar Obelisk and in the non-host grass species *B. distachyon* were evaluated after 4 DPI. They found that genes encoding proteins with putative secretion signals were enriched among those up-regulated during infection of wheat and genes with plant-specific expression patterns. In our analysis, we observe a higher proportion of small, secreted proteins (SSPs) in the up-regulated sets of genes at 1 and 3 DPI compared to the down-regulated sets.

Among the 31 selected effector candidates, an interesting finding is that effector candidate Mycgr3109710 localizes to the nucleus and labels mobile cytosolic bodies that are predominantly located at the cell periphery when expressed in *Nicotiana*. This effector candidate is annotated as a member of the Allergen V5/Tpx-1 related group, which are cysteine-rich secretory proteins (Crips) including proteins of the PR-1 family and potent allergens (Wangorsch et al., 2022). Protein feature analysis using InterProScan revealed cystine-rich secretory proteins, antigen 5, and pathogenesis-related 1 proteins (CAP) and sperm-coating protein (SCP) domains in Mycgr3109710, indicating its association with the homologous PR-1-like superfamily. Additionally, a BLAST search identified significantly similar PR-1-like proteins in *Zymoseptoria brevis* and *Aureobasidium* sp. While research on non-plant PR-1-like proteins has primarily focused on humans and animals, there have been limited studies in filamentous ascomycetes. In *Fusarium graminearum*, a recent study characterized four PR-1-like proteins; deletion of one of these resulted in reduced fungal virulence (Lu & Edwards, 2018). Furthermore, the hemibiotrophic pathogens *Moniliophthora perniciosa* and *M. roreri* possess a significant number of PR-1-like genes, many of which are up-regulated during biotrophic interactions with the cacao host plant (Teixeira et al., 2012). This coincides with the expression that we observed for Mycgr3109710 at the early infection stage (1 and 3 DPI). We hypothesize that Mycgr3109710 targets a component or protein in the vesicle-trafficking system of the plant. We base this proposition on the similar subcellular localization pattern of PR-1 variants from *Arabidopsis thaliana* expressed in *N. benthamiana* plants (Pečenková et al., 2022) to mobile punctate structures. In their analysis, the PR1-GFP construct is localized to multivesicular bodies (MVB) and the extracellular space.

Similarly, Mycgr394290 localizes to the nucleus and labels cytosolic punctate structures with less mobility than those labeled by Mycgr3109710. We suggest that Mycgr394290 may target organelles involved in sorting and trafficking of molecules. An example of a fungal effector with similar localization is Foa3 from *Fusarium oxysporum*, which functions within the plant cell to suppress host defenses. Foa3 showed a weak signal in the cytosol but was strongly detected in punctate structures when a secretory signal peptide was included (Tintor et al., 2022). These punctate structures resemble the cytosolic bodies labeled by Mycgr394290:sYFP in our study. Regarding their identity, Tintor et al. (2022) proposed that the labeled structures may represent vesicles containing proteins targeted for secretion. Furthermore, their study demonstrates that Foa3 suppresses pattern-triggered defense responses to the same extent regardless of whether the protein carries the signal peptide (Tintor et al., 2022). This is intriguing because Mycgr394290 encodes predicted mitochondrial, chloroplast, and nuclear localization signals according to LOCALIZER (Table 4). Although the exact identity of the punctate subcellular structures labeled by Mycgr394290:sYFP is uncertain, it is plausible that this protein acts to suppress the plant's defense mechanisms in the same way as Foa3, which is known to suppress the plant immune response.

Another candidate effector, Mycgr3107904, was mainly localized to the cytosol. This effector is annotated as a Hce2 domain-containing protein. Hce2 (named from **h**omologs of ***C****. fulvum* **E**cp2 effector) is a domain that causes plant cell death, and is widely conserved in the fungal kingdom (Laugé et al., 1997; Zhang et al., 2019). There are three predicted Hce2-containing effectors in the genome of *Z. tritici*: MgEcp2 (Mycgr3104404), MgEcp2-2 (Mycgr3107904) and MgEcp2-3 (Mycgr3111636) (Stergiopoulos et al., 2010, 2012). In addition, a fourth homolog of Ecp2 was found to be up-regulated in *Z. tritici* at 8 DPI and then down-

regulated at 12 DPI. This effector candidate induces necrosis in wheat in a cultivar-dependent manner (Ben et al., 2015). In another study (Mirzadi Gohari et al., 2015), Mycgr3104404, Mycgr3107904 and Mycgr3111636 were up-regulated during the transition to necrotrophy, and in the necrotrophic stage at 8 and at 12 dpi. In our study, Mycgr3111636 was up-regulated at 1 DPI and at 10 DPI but we were unable to transform this effector candidate into *Agrobacterium*, suggesting a possible toxic effect on *Agrobacterium* cells. We transformed Mycgr3107904, which was up-regulated at 10 DPI, and we found that the fluorescence signal was mainly localized to the cytosol. This is very interesting as the Ecp effector of *C. fulvum* is one of the few proteins that can induce necrosis in tomato and tobacco plants irrespective of the signal peptide, which indicates that its host target is intracellular (Ben et al., 2015). We did not observe fluorescence in a specific intracellular compartment but the protein is localized within the cytosol, which suggests a plausible intracellular target protein in the plant.

In our analyses Mycgr3111221 and Mycgr3105487, which are Lysin (LysM) domain-containing effectors, were up-regulated at the early stage of infection. There are three LysM effector genes identified and characterized in the *Z. tritici* genome (Marshall et al., 2011; Sánchez-Vallet et al., 2020; Tian et al., 2021). Two of them, Mycgr3111221 and Mycgr3105487, were previously shown to be up-regulated during the asymptomatic phase (Marshall et al., 2011; Tian et al., 2021). Interestingly, Mycgr3111221 suppresses chitin-induced plant immunity, and both effectors were able to protect fungal hyphae against plant chitinase activity (Marshall et al., 2011). These LysM effectors in *Z. tritici* are homologous of the Ecp6 effectors in *C. fulvum*, which are secreted directly into the apoplastic space where they perform their chitin-binding function (Sánchez-Vallet et al., 2020). In our analysis, these effectors also were up-regulated at the early (presymptomatic) stage of infection. Both effector candidates are localized to the

nucleus and cytosol. This might be due to a dual targeting function where the effectors have a primary localization in the apoplast, but also can interact with host targets in the cytosol. Alternatively, this could be because all effectors are initially delivered into the apoplast and may have a virulence function in the apoplastic space, but others can be also translocated from the apoplast to the plant cell cytosol, where they can perform other virulence functions in a specific cell compartment (Rocafort et al., 2020).

Two additional effector candidates, Mycgr339947 and Mycgr3111223, possess compelling annotations. Mycgr339947 is annotated as a cerato-platanin, but despite our efforts, we encountered challenges in obtaining transformed colonies of *Agrobacterium* carrying Mycgr339947. Mycgr3111223 is annotated as a heat-shock protein with a DnaJ domain and exhibits localization in both the nucleus and cytosol. The DnaJ domain in Mycgr3111223 is a member of the Hsp40 family of molecular chaperones which are known for regulating the activity of Hsp70s. Hsp70s are involved in folding of proteins, coordination of responses to stress, and targeting selected proteins for degradation. In *Pseudomonas syringae* pv. *maculicola,* HopI1 is an effector protein with a C-terminal region with homology to a J domain found in Hsp40. This effector localizes to chloroplasts during expression in plants and targets chloroplast Hsp70 to promote bacterial virulence by suppressing plant defenses and salicylic acid (SA) accumulation (Jelenska et al., 2007). This is not consistent with the nuclear and cytosolic localization seen for Mycgr3111223 in our study. However, in an experiment that overexpressed a type-III DnaJ domain-containing Hsp40 from *Glycine max* (soybean) in *N. benthamiana*, the Hsp40 from soybean was highly induced during infection by rust. The overexpression of Hsp40 in *N. benthamiana* caused a hypersensitive response (HR)-like cell death that was dependent on the nuclear localization of the effector protein, and which coincides with the presence of a

predicted NLS. In *Z. tritici*, it has been previously suggested that the fungus is able to hijack the immune system and hyperactivate the induced cell-death response from the plant to improve colonization by the pathogen (Rudd et al., 2015). It is plausible that *Z. tritici* is activating an effector protein with a similar function to that of Hsp40 in activating a hypersensitive response through interaction with Hsp70s in the plant. The induction of an HR-like response caused by Mycgr3111223 needs to be assessed in future experiments in *N. benthamiana* to test this hypothesis.

In summary, we characterized the fungal transcriptome response during compatible, incompatible and non-host interactions. We have successfully identified crucial time points during the infection process where *Z. tritici* dynamically regulates sets of genes. In addition, we conducted pathway and gene function enrichment analysis for each type of interaction, compatible, incompatible, and non-host. Notably, we identified 31 effector candidates that are expressed early in infection, and two of them during the transition to the necrotrophic stage. The predicted effectors exhibit intriguing subcellular localizations, including the nucleus, cytosol, and mobile cytosolic bodies, suggesting their potential involvement in vesicle-trafficking mechanisms. Our findings contribute to the understanding of effector candidates in *Z. tritici* and shed light on new functional roles that have yet to be characterized. Future investigations will address whether the effector candidates identified in our study have a functional role in fungal pathogenicity as well as suppress immune responses in wheat.

Materials and Methods

Plant material and inoculum preparation.

Highly susceptible wheat cultivar Taichung 29, R-gene resistant cultivars Veranopolis and Israel 493, and the non-host barley cultivar Kindred were grown in a greenhouse in Metro-mix 500 series potting soil (SunGro Horticulture, Bellevue, WA), with a constant 16 h light and 8 h dark cycle for 2-3.5 weeks. Wheat and barley were planted in three biological replicates consisting of 3 plants per 4-inch pot. A 1 cm^2 piece of lyophilized filter paper stock (stored at -80) of isolate IPO323 of *Z. tritici* was placed into 100 ml of yeast-sucrose broth with 100 µl of kanamycin sulfate (25 mg/ml). The flask was placed on a shaker at 25ºC for 3 days. The inoculum concentration was adjusted to $1.0x10^6$ conidia/ml, and 1 µl of Tween 20 (polysorbate 20) was added per 100 ml of inoculum. The inoculum was hand sprayed evenly over 14-days-old (2nd-3rd leaf stage) wheat and barley plants. Inoculated plants were enclosed in a humidity chamber draped in plastic and muslin for 72 h, then removed to normal growth chamber conditions for the duration of the experiment. Emerging leaves of wheat and barley were trimmed every 2-3 days to ensure that the inoculated leaves remained "healthy" and that only inoculated tissue was harvested.

Nicotiana benthamiana was grown in Berger Seed Germination and Propagation Mix supplemented with Osmocote slow-release fertilizer (14-14-14). Plants were maintained in a growth chamber with a 16h:8h light:dark photoperiod at 24°C with light and 22°C in the dark and 60% humidity with average light intensities at plant height of 130 µmols/m^2/s.

RNA extraction and sequencing

Wheat and barley leaf tissue was harvested by clipping 2 leaves per plant per replicate and bulking 3 plants per replicate. Leaf tissue was harvested at 1, 3, 6, 10, 17 and 23 days post inoculation (DPI). All harvested leaf material was immediately frozen in liquid nitrogen. RNA was extracted using the RNeasy Plant Mini kit (Qiagen). For each replicate 1 µg of total RNA

was used to produce cDNA libraries (Purdue Genomics Core Facility, West Lafayette, IN) for RNA sequencing. The sequencing was done using Illumina HiSeq paired-end (PE) 100 base-pair reads. Read quality was checked with FastQC (Andrews, 2010) before and after trimming to remove low-quality and residual adapter sequence (Trimmomatic v.0.36). All reads were mapped to the reference genome of the *Z. tritici* IPO323 strain (*M. graminicola* v.2.0) retrieved from the Joint Genome Institute (JGI) (Goodwin et al., 2011) using BBMap **(**v 35.85; Bushnell B., sourceforge.net/projects/bbmap/). Reads mapped to the reference genome were counted using HTSeq (Anders et al., 2015). Fewer read counts were detected in all the samples of the non-host interaction, and in the samples of the incompatible interactions at 17 and 23 DPI compared to the samples of the compatible interaction, due to the reduced fungal growth in the resistant wheat cultivars at the late stage and in the non-host species barley. As a result, for the comparisons of compatible versus incompatible interactions, and compatible versus non-host interactions, we removed from the whole dataset the genes that did not have any measurable counts in the replicates of the incompatible and non-host interactions at specific time points. This allowed us to improve the normalization of the counts and the consistency between replicates. This approach reduced the total number of DEGs that we were able to find at each time point, but we could accurately detect significant differences in the highly expressed genes in the samples and reduce the false positives. We encountered limitations in the analysis due to the low read counts obtained in the replicates of the incompatible interactions and non-host interaction. These limitations include reduced sensitivity in detecting low-abundance transcripts or less expressed genes in the pathogen, and difficulty in assigning functional annotations or representative GO terms for some sets of DEGs.

Data were normalized and filtered using the R package DESeq2 v.4.0.3 (Love et al., 2014), which uses the median of ratios method to determine the size factors and the shrinkage method for variance estimation. The normalization for the comparison of compatible versus incompatible interactions was conducted on two groups of samples. One group contains the samples at 1, 3, 6 and 10 DPI, and the other group contains the samples at 17 and 23 DPI. We used this approach because very few reads were detected in the samples of the incompatible interaction at 17 and 23 DPI obtaining many genes with not measurable expression. Similarly, in the comparison of compatible and incompatible interactions versus the non-host host interaction, the normalization was conducted on one group that contains the samples from 1 and 3 DPI, a second group of samples from 6 and 10 DPI, and a third group that contains the samples at 17 and 23 DPI. Differential gene expression analysis for the pathogen between inoculation treatment samples within each 6-point time course was completed using DESeq2 v.4.0.3 (Love et al., 2014). Significant DEGs were determined at FDR = 5% and using a cutoff of 1-fold change in expression between comparisons.

GO and KEGG pathway enrichment analysis.

The differentially expressed genes (DEGs) were subjected to Gene Ontology (GO) enrichment analysis using gProfiler (Raudvere et al., 2019). *Mycosphaerella graminicola* v.2.0 genes with detectable counts in our analysis were used as the background reference for *Z. tritici*. The significance threshold was determined by the default gProfiler method, the g:SCS method, which corresponds to an experiment-wide threshold of $\alpha = 0.05$ (Raudvere et al., 2019). KOBAS v.3.0. (Bu et al., 2021) supports *Z. tritici* and was used to calculate KEGG pathway enrichment (Kanehisa et al., 2017) of the significantly expressed genes; significance was determined by

using Fisher's exact test (Fisher, 1925) using the Benjamini and Hochberg method to correct for multiple testing (Benjamini and Hochberg 1995).

Selection of candidate effectors from *Z. tritici*.

Effector predictions were performed as previously described by Helm et al. (2022) with modifications. We used SignalP (v6.0) (Teufel et al., 2022) and Phobius (v1.01) to predict signal peptide sequences and we applied a probability threshold of 0.9. The absence of transmembrane domains was predicted using Phobius (v1.01) (Käll et al., 2004) and DeepTMHMM (v1.0.24**)** (Hallgren et al., 2022). EffectorP (v.3.0) (Sperschneider & Dodds, 2022) was used to select *Z. tritici* proteins that contained effector-like sequence characteristics. LOCALIZER (v.1.0.4) (Sperschneider et al., 2017) and ApoplastP (v.1.0) (Sperschneider et al., 2018) were used to predict the possible localization of the candidate effectors. The list of *Z. tritici* putative effectors is shown in Table 4.

Generation of plant expression constructs.

Constructs were generated using a modified multisite Gateway cloning (Invitrogen) strategy (Helm et al., 2022; Qi et al., 2012). The 3xHA:sYFP (free super yellow fluorescent protein) construct has been described previously (Helm et al., 2022; Jaiswal et al., 2023).

The attL1 and attL4 Gateway recombination sequences were fused to the 5' and 3' ends of the open reading frames (ORFs) of each *Z. tritici* candidate effector, thereby generating Gateway-compatible donor clones. A commercial gene synthesis company (Azenta Life Sciences) was used to synthesize each candidate effector (without the predicted signal peptides) and the sequences were inserted into the pUC57 plasmid by the service provider and designated pDONR(L1-L4):ZtEC..

To generate the ZtEC:sYFP protein fusions, the pDONR(L1-L4):ZtEC constructs were mixed with pBSDONR(L4r-L2):sYFP (Helm et al., 2022; Qi et al., 2012) and recombined into the plant expression plasmid pEG100 (Earley et al., 2006) using LR Clonase II (Invitrogen) following the manufacturer's instructions. The resulting constructs were verified by sequencing and subsequently used for transient expression assays.

Agrobacterium-mediated transient protein expression in _N. benthamiana_.

Agrobacterium-mediated transient expression was performed as described previously (Helm et al., 2022) with modifications. The constructs described above were mobilized into *Agrobacterium tumefaciens* strain GV3101 (pMP90) and grown in Luria-Bertani (LB) broth supplemented with 25 µg of gentamicin sulfate and 50 µg of kanamycin per milliliter at 30°C for two days. Transformants were inoculated into 10 mL of liquid LB containing the appropriate antibiotics and were shaken overnight at 30°C at 250 rpm. Following overnight incubation, the cells were pelleted by centrifuging at 3,800 rpm for 3 minutes and resuspended in 10 mM $MgCl_2$. The bacterial suspensions were adjusted to an optical density at 600 nm (OD_{600}) of 0.5 and incubated with 100 µM acetosyringone for 3-4 hours at room temperature prior to agroinfiltration. Bacterial suspensions were infiltrated into the abaxial surface of 3- to 4-week-old *N. benthamiana* leaves with a needleless syringe.

Laser scanning confocal microscopy.

Live-cell imaging of *N. benthamiana* epidermal cells was performed forty-eight hours post-agroinfiltration using a Zeiss LSM880 Axio Examiner upright confocal microscope equipped with a Plan Apochromat 20x/0.8 objective (pinhole 1.0 AU). The sYFP-tagged fusion proteins were excited using a 514-nm argon laser, and fluorescence signals were detected

between 517 nm and 562 nm. All confocal micrographs were processed using the Zeiss Zen Blue Lite program. Image analysis was performed using the Fiji plugin of Image J 2.0.0 (http://fiji.sc/Fiji).

Immunoblot analyses.

Immunoblot analyses were performed as described previously with slight modifications (Helm et al., 2022; Jaiswal et al., 2023). Nine leaf discs of *N. benthamiana* (0.15 g per sample) were collected at 48 hours after agroinfiltration and flash frozen in liquid nitrogen. Frozen tissue was homogenized with 2 volumes of protein extraction buffer (150 mM NaCl, 50 mM Tris [pH 7.5], 0.1% Nonidet P-40 [Sigma-Aldrich], 1% plant protease inhibitor cocktail [Sigma-Aldrich], and 1% 2,2'-dipyridyl disulfide) using a cold ceramic mortar and pestle. The solution was centrifuged at 13,000 x g for 15 minutes at 4°C. Seventy-five microliters of the collected supernatants were combined with 25 uL of 4x Laemmli Buffer (BioRad) supplemented with beta-mercaptoethanol. Total protein samples were separated on a 4-20% Tris-glycine stain-free polyacrylamide gel (BioRad) at 180 V for 1 hour in 1x Tris/glycine/SDS running buffer. Total proteins were transferred to a nitrocellulose membrane and subsequently blocked in 5% skim milk for 1 hour at room temperature. Horseradish peroxidase-conjugated anti-GFP antibody (1:5,000) (Miltenyi Biotec) was used to detect sYFP-tagged recombinant proteins. Immunoblots were incubated for 5 minutes at room temperature with Supersignal West Femto maximum sensitivity substrates (Thermo Scientific) and developed using an ImageQuant 500 CCD imaging system (Cytiva).

Acknowledgments

The authors thank Drs. Terri Cameron and Ian Thompson (USDA-ARS, Crop Production and Pest Control Research Unit) for technical assistance and the Purdue University Imaging Facility for access to the Zeiss LSM880 Axio Examiner upright confocal microscope. The funding bodies had no role in designing the experiments, collecting the data, or writing the manuscript. All opinions expressed in this paper are the authors' and do not necessarily reflect the policies and views of USDA. USDA is an equal opportunity provider and employer.

Funding

This research was funded by the United States Department of Agriculture, Agricultural Research Service (USDA-ARS) research project 5020-21220-014-00D.

TABLES

Table 1. Comparisons of gene expression by the wheat pathogen *Zymoseptoria tritici* during compatible (susceptible) and incompatible (R-gene) interactions on wheat and its non-host interaction on barley.

Species and cultivar inoculated		
Test	**Versus**	**Comparison**
Wheat, Taichung 29	Wheat, Veranopolis (*Stb2*)	Compatible vs. R-gene
	Wheat, Israel 493 (*Stb3*)	Compatible vs. R-gene
	Barley, Kindred	Compatible vs. Non-host
Wheat, Veranopolis (*Stb2*)	Wheat, Israel 493 (*Stb3*)	R-gene vs. R-gene
Barley, Kindred	Wheat, Veranopolis (*Stb2*)	Non-host vs. R-gene
	Wheat, Israel 493 (*Stb3*)	Non-host vs. R-gene

Table 2. Differentially expressed genes of the wheat pathogen *Zymoseptoria tritici* when comparing susceptible (compatible) versus two incompatible (R-gene) interactions.

	R gene (*Stb2*) – R gene (*Stb3*)[a]	**Compatible - R gene (*Stb2*)[b]**	**Compatible-R gene (*Stb3*)[c]**

Time point[d]	**1**	**3**	**6**	**10**	**17**	**23**	**1**	**3**	**6**	**10**	**17**	**23**	**1**	**3**	**6**	**10**	**17**	**23**
Up[e]	0	0	1	1	13	3	0	1	12	275	21	33	1	0	21	226	34	34
Down[e]	0	0	0	11	1	0	0	4	0	326	11	23	1	4	0	361	13	22
Total DEGs	0	0	1	12	14	3	0	5	12	601	32	56	2	4	21	587	47	56
Total detectable genes	1,504				222		1,504				222		1,504				222	

[a] Responses of *Z. tritici* isolate IPO323 when grown on *Stb2*-resistant plants of cultivar Veranopolis compared to those on *Stb3*-resistant plants of cultivar Israel 493
[b] Responses of *Z. tritici* isolate IPO323 when grown on susceptible cultivar Taichung 29 compared to those on *Stb2*-resistant plants of cultivar Veranopolis
[c] Responses of *Z. tritici* isolate IPO323 when grown on susceptible cultivar Taichung 29 compared to those on *Stb3*-resistant plants of cultivar Israel 493
[d] 6-point time course. Time points are measured in days after inoculation.
[e] Significantly differentially expressed genes that are up- or down-regulated at a False Discovery Rate (FDR) of 5%.

Table 3. Differentially expressed genes of the wheat pathogen *Zymoseptoria tritici* when comparing susceptible (compatible) and incompatible (R-gene) interactions versus non-host interaction on barley.

	Compatible– Non-host[a]						**R gene (*Stb2*) – Non-host[b]**						**R gene (*Stb3*) - Non-host[c]**					
Time Point[d]	**1**	**3**	**6**	**10**	**17**	**23**	**1**	**3**	**6**	**10**	**17**	**23**	**1**	**3**	**6**	**10**	**17**	**23**
Up[e]	74	124	43	94	57	63	67	107	40	68	20	30	68	108	54	70	9	22
Down[e]	40	47	48	52	14	17	40	47	44	41	9	27	41	52	59	39	9	23
Total DEGs	114	171	91	146	71	80	107	154	84	109	29	57	109	160	113	109	18	45
Total detectable genes	284		352		107		284		352		107		284		352		107	

[a] Responses of *Z. tritici* isolate IPO323 when grown on plants of susceptible wheat cultivar Taichung 29 compared to those on non-host barley plants
[b] Responses of *Z. tritici* isolate IPO323 when grown on *Stb2*-resistant plants of cultivar Veranopolis compared to those on non-host barley plants
[c] Responses of *Z. tritici* isolate IPO323 when grown on *Stb3*-resistant plants of cultivar Israel 493 compared to those on non-host barley plants
[d] 6-point time course. Time points are measured days after inoculation.

[e] Significantly differential expressed genes that are up- or down-regulated at a False Discovery Rate (FDR) of 5%.

Table 4. Characteristics of *Zymoseptoria tritici* candidate effectors selected for further analysis

ID	Amino acids	Signal peptide	Protein size (kDa)	LOCALIZER prediction	Annotation
Mycgr394290	184	18-19	18.61	Chloroplast (95-118) Mitochondria (68-88) NLS	Uncharacterized
Mycgr3111221	232	16-17	22.43		Peptidoglycan-binding LysM
Mycgr3106502	89	18-19	8.01		Uncharacterized
Mycgr3104794	157	20-21	15.15		Uncharacterized
Mycgr3109991	235	20-21	24.87	NLS	Uncharacterized
Mycgr3105487	97	18-19	8.7		Peptidoglycan-binding LysM
Mycgr3109710	200	26-27	18.8		Allergen V5/Tpx-1 related
Mycgr3106125	70	23-24	4.95		Uncharacterized
Mycgr3111223	554	18-19	58.81		Heat shock protein DnaJ, N-terminal
Mycgr3110220	131	19-20	12.88		Uncharacterized
Mycgr3107904	170	23-24	15.65		Hce2 domain-containing protein

Mycgr346866	427	22-23	41.15		Carbohydrate kinase, PfkB
Mycgr383064	75	18-19	6.15		Uncharacterized
Mycgr3102792	114	19-20	10.63	NLS	Uncharacterized
Mycgr379161	68	19-20	4.98		Uncharacterized
Mycgr3106106	140	20-21	14.44		Uncharacterized
Mycgr3111636	159	19-20	14.63		Hce2 domain-containing protein
Mycgr3109137	154	18-19	15.81		Uncharacterized
Mycgr3102996	163	23-24	15.12		Uncharacterized
Mycgr3110887	283	19-20	30.59		Uncharacterized
Mycgr3104009	483	25-26	51.39		Beta-Ig-H3/fasciclin
Mycgr339947	149	17-18	13.95		Cerato-platanin
Mycgr3105223	188	23-24	18.19		Uncharacterized
Mycgr3105182	143	18-19	13.88		Uncharacterized
Mycgr3104697	149	19-20	13.49		Uncharacterized
Mycgr3101652	77	21-22	6.06		Uncharacterized
Mycgr3106456	193	30-31	16.59	Chloroplast (27-65)	GPI-anchored domain-containing protein
Mycgr3106329	135	19-20	13.06		Uncharacterized

Mycgr382936	155	20-21	13.97	Plastocyanin-like
Mycgr399161	164	15-16	16.03	Uncharacterized
Mycgr3102849	285	20-21	27.95	Uncharacterized

FIGURES.

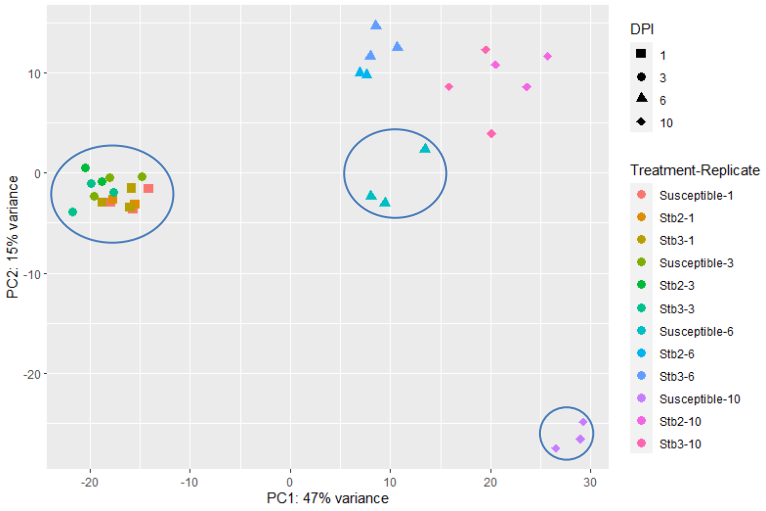

Fig 1.

Principal component analysis (PCA) of the normalized and filtered counts for RNA sequencing reads of *Zymoseptoria tritici* inoculated onto the highly susceptible wheat cultivar Taichung 29 (Susceptible) or the R-gene-containing resistant wheat cultivars Veranopolis (*Stb2*) or Israel 493 (*Stb3*) at 1, 3, 6, and 10 days post inoculation (DPI). Circles represent cluster 1 (DPI 1 and 3), cluster 2 (DPI 6), and cluster 3 (DPI 10) that contain the replicates of the compatible interaction.

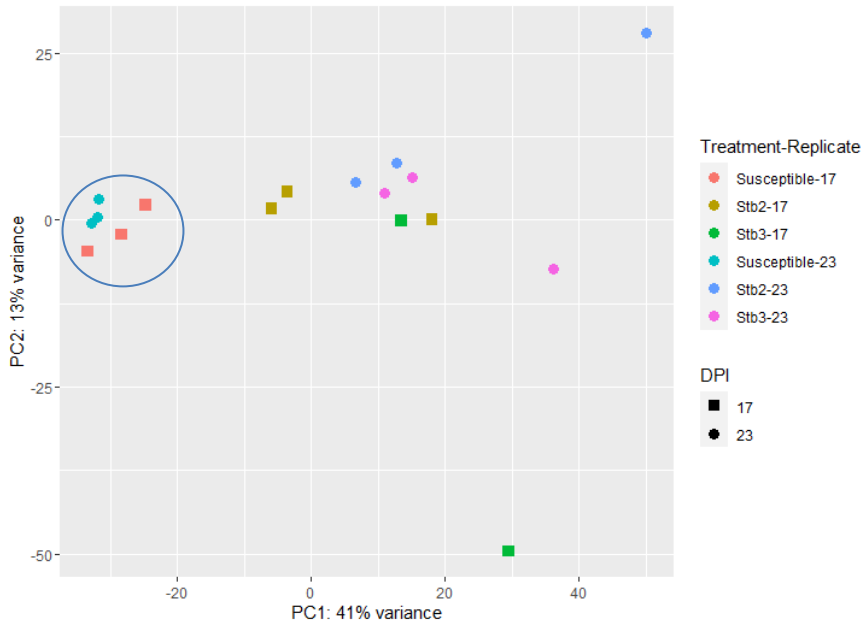

Fig 2.

Principal component analysis (PCA) of the normalized and filtered counts for RNA sequencing reads of *Zymoseptoria tritici* inoculated onto the highly susceptible wheat cultivar Taichung 29 (Susceptible) or the R-gene-containing resistant wheat cultivars Veranopolis (*Stb2*) or Israel 493 (*Stb3*) at 17 and 23 days post inoculation (DPI). Circle represents cluster 4 (DPI 17 and 23) that contains the replicates of the compatible interaction.

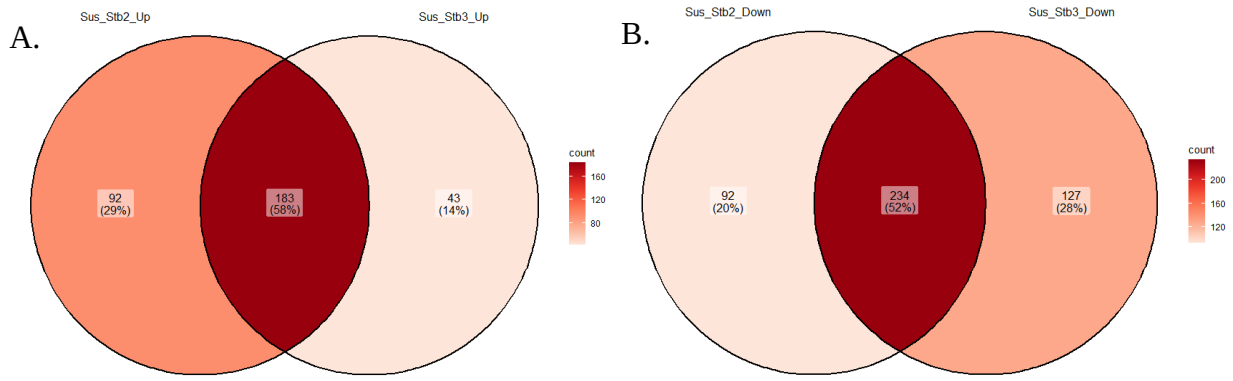

Fig 3.

Venn diagrams showing common and unique differentially up-regulated (A) and down-regulated (B) genes of *Zymoseptoria tritici* at 10 days post inoculation (DPI) between the compatible interaction and the two R-gene interactions on wheat.

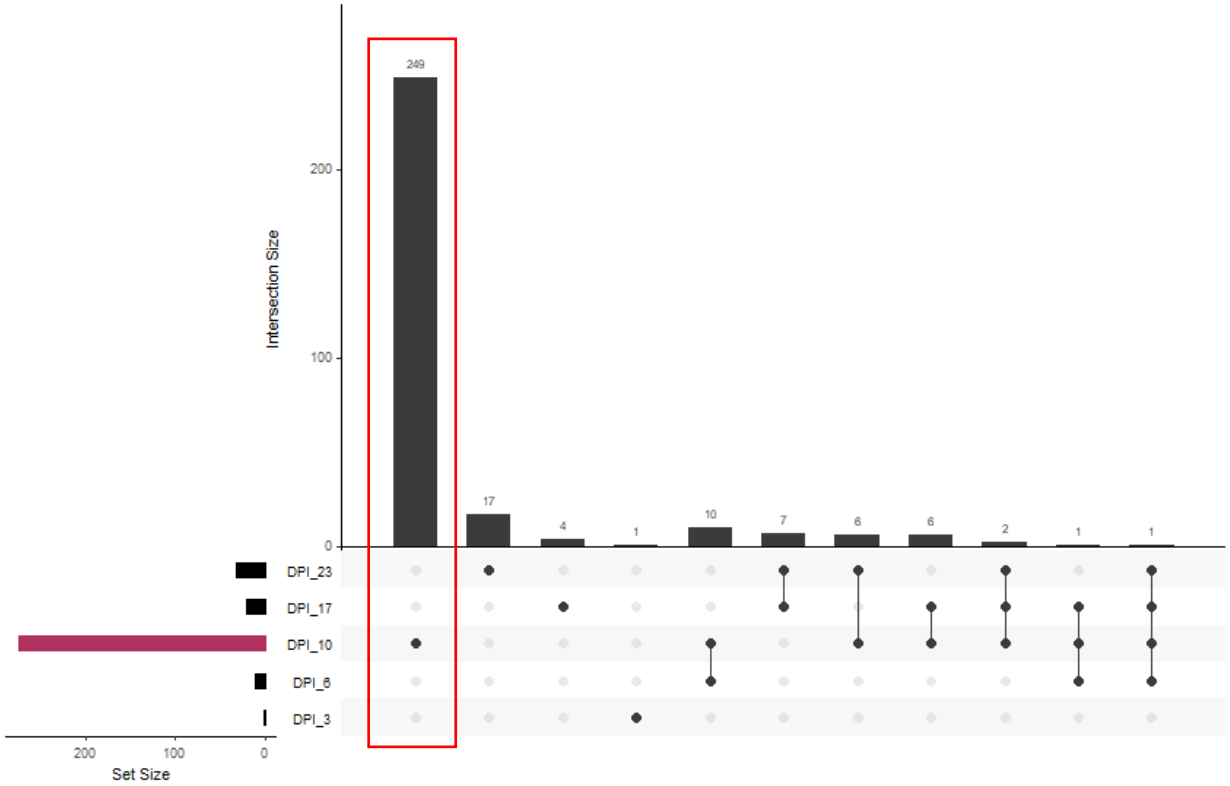

Fig. 4.

Numbers of unique and shared up-regulated differentially expressed genes (DEGs) of the wheat pathogen *Zymoseptoria tritici* during the compatible interaction on the highly susceptible cultivar Taichung 29 compared to the incompatible interaction on the *Stb2*-carrying cultivar Veranopolis at 3, 6, 10, 17 and 23 days post inoculation (DPI). The colored horizontal bar represents the time point at which the highest number of unique up-regulated DEGs was observed.

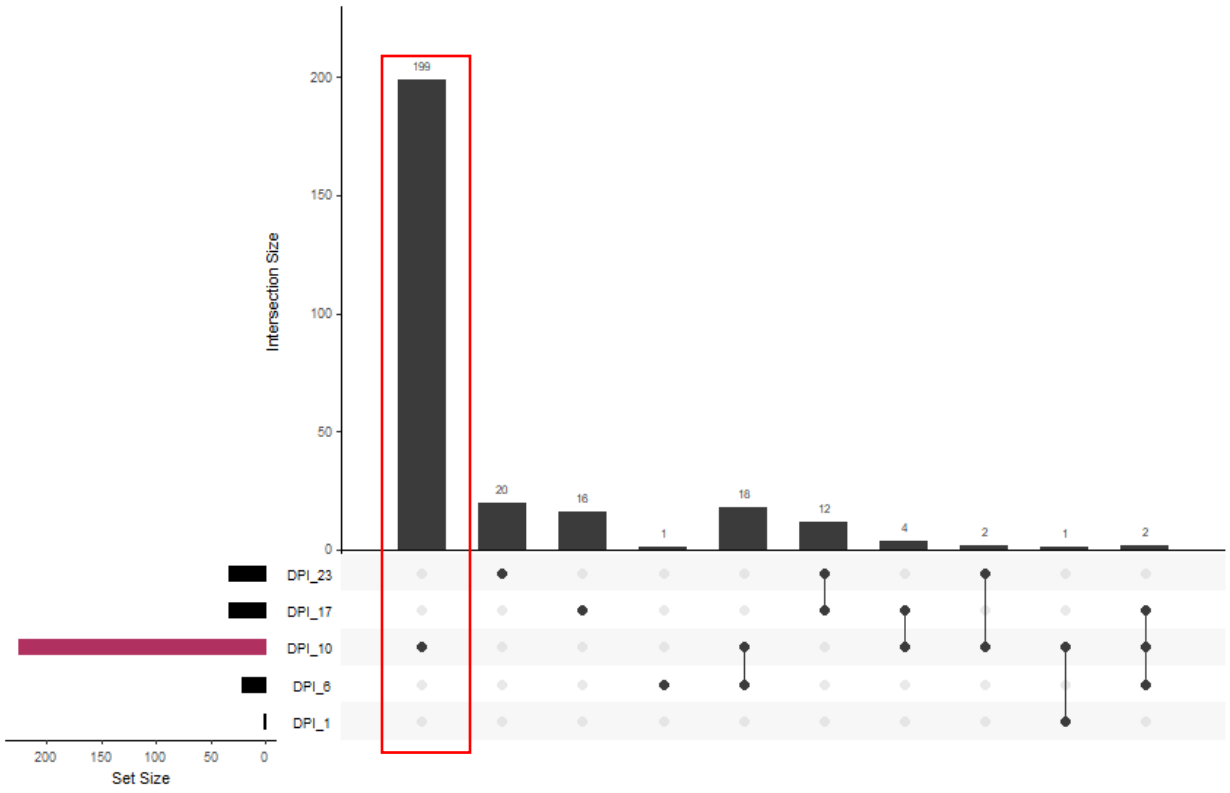

Fig. 5.

Numbers of unique and shared up-regulated differentially expressed genes (DEGs) of the wheat pathogen *Zymoseptoria tritici* among six time points during the compatible interaction on cultivar Taichung 29 compared to the incompatible interaction on the *Stb3*-carrying cultivar Israel 493. The colored horizontal bar represents the time point at which the highest number of unique up-regulated DEGs was observed.

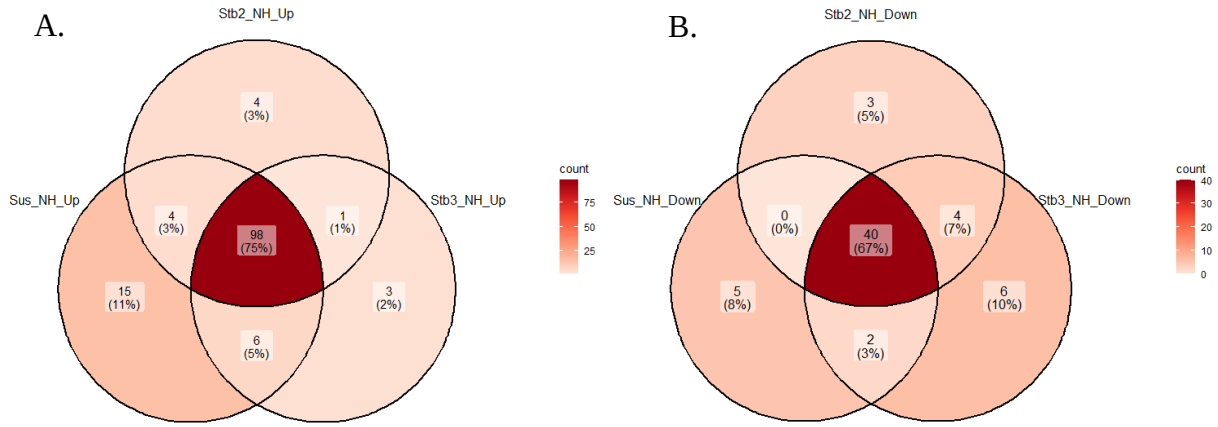

Fig. 6.

Venn diagrams showing common and unique differentially up-regulated (A) and down-regulated (B) *Zymoseptoria tritici* genes at 3 days post inoculation between the compatible and the two R-gene interactions on wheat compared to the non-host interaction on barley.

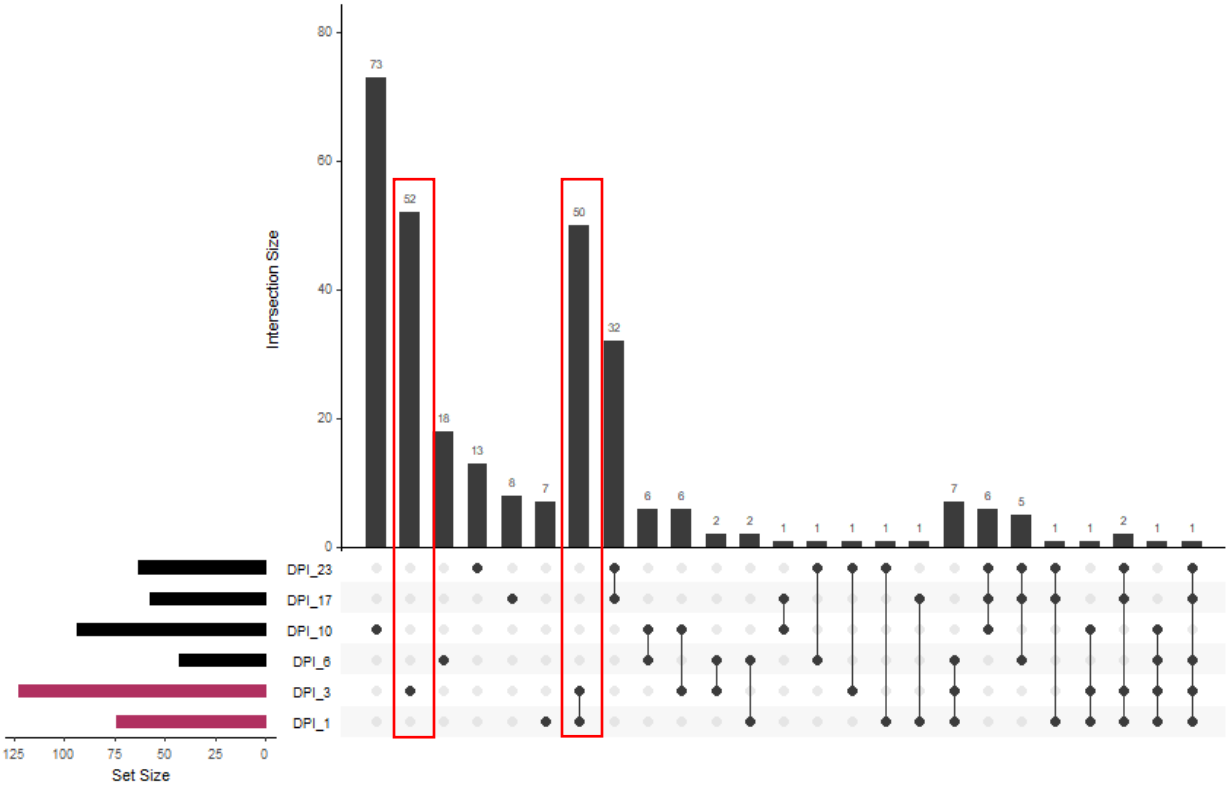

Fig. 7.

Numbers of unique and shared up-regulated differentially expressed genes (DEGs) of the wheat pathogen *Zymoseptoria tritici* among six time points during the compatible interaction on wheat cultivar Taichung 29 compared to its non-host interaction on barley. The colored horizontal bars represent the time points at which the highest number of unique up-regulated DEGs was observed.

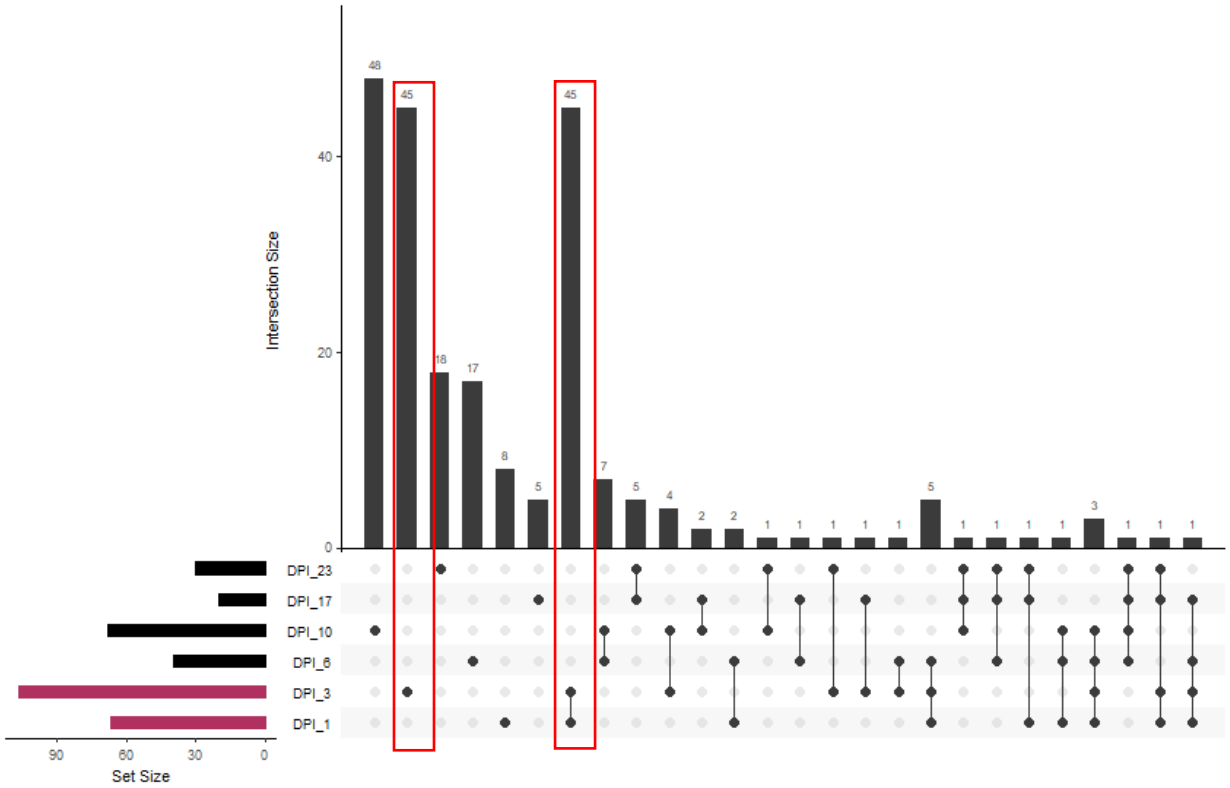

Fig. 8.

Numbers of unique and shared up-regulated differentially expressed genes (DEGs) of the wheat pathogen *Zymoseptoria tritici* among six time points during the R-gene interaction on *Stb2*-carrying wheat cultivar Veranopolis compared to its non-host interaction on barley. The colored

horizontal bars represent the time points at which the highest number of unique up-regulated DEGs was observed.

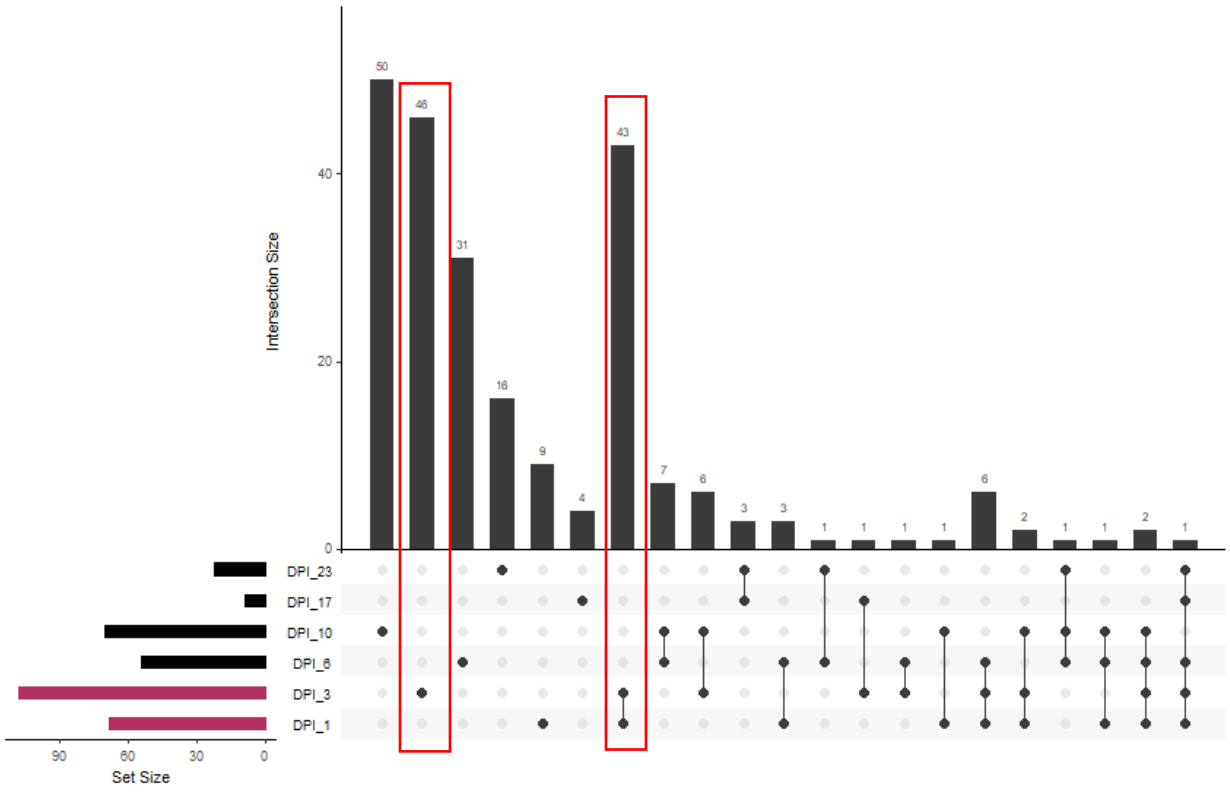

Fig. 9.

Numbers of unique and shared up-regulated differentially expressed genes (DEGs) of the wheat pathogen *Zymoseptoria tritici* among six time points during the R-gene interaction on *Stb3*-carrying wheat cultivar Israel 493 compared to its non-host interaction on barley. The colored horizontal bars represent the time points at which the highest number of unique up-regulated DEGs was observed.

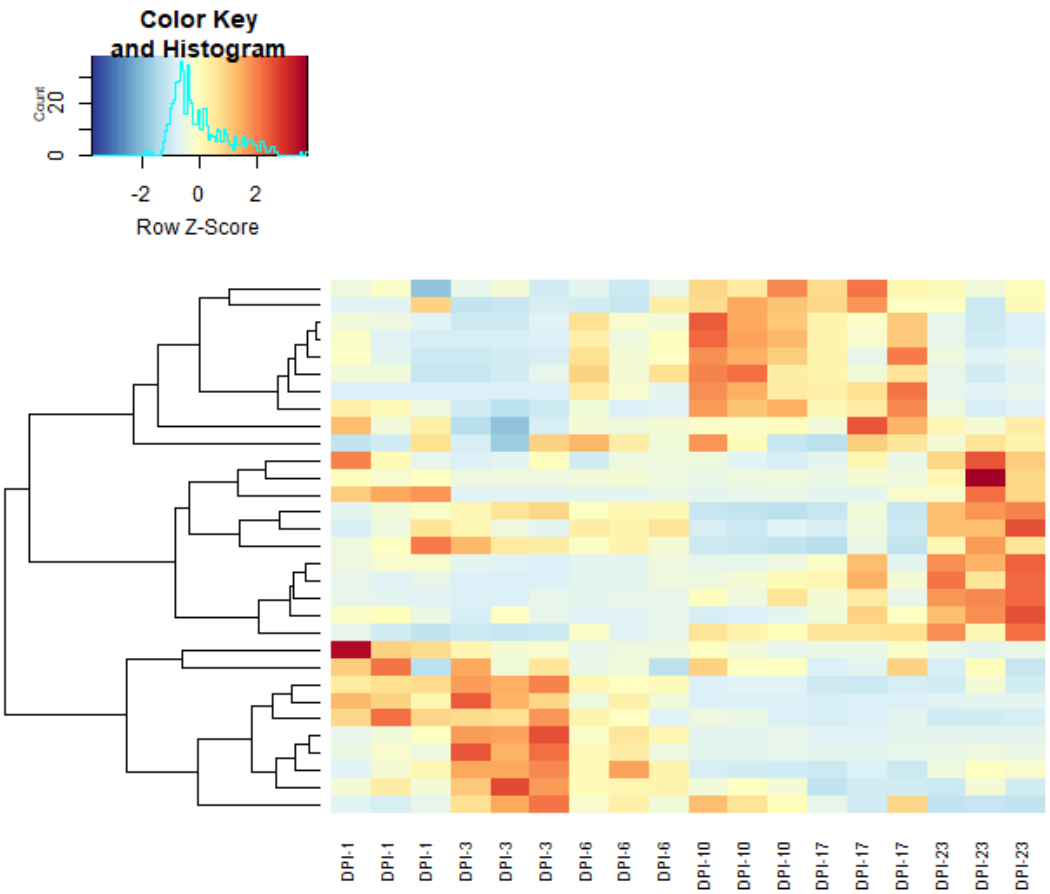

Fig. 10.

Relative expression of 31 selected *Zymoseptoria tritici* effector candidates. Heat map shows the normalized expression value of each effector candidate in the individual samples for each time point. The dendrogram on the left shows the clustering of the candidate effectors based on the relative expression calculated by the Pearson correlation.

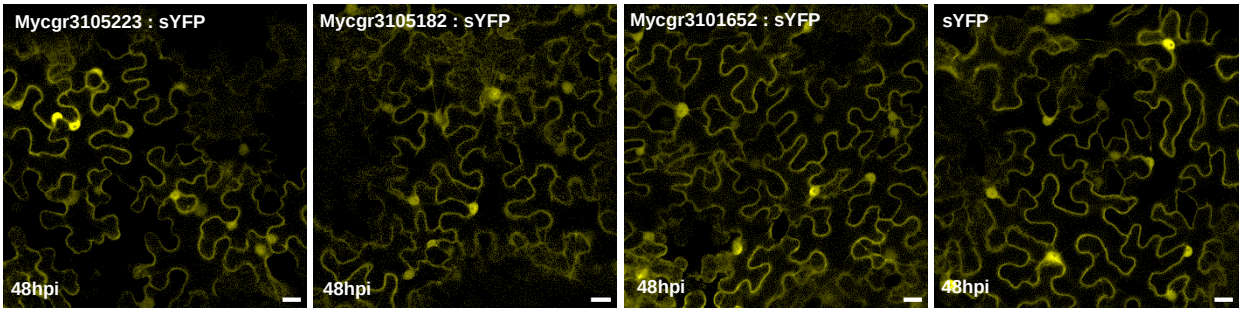

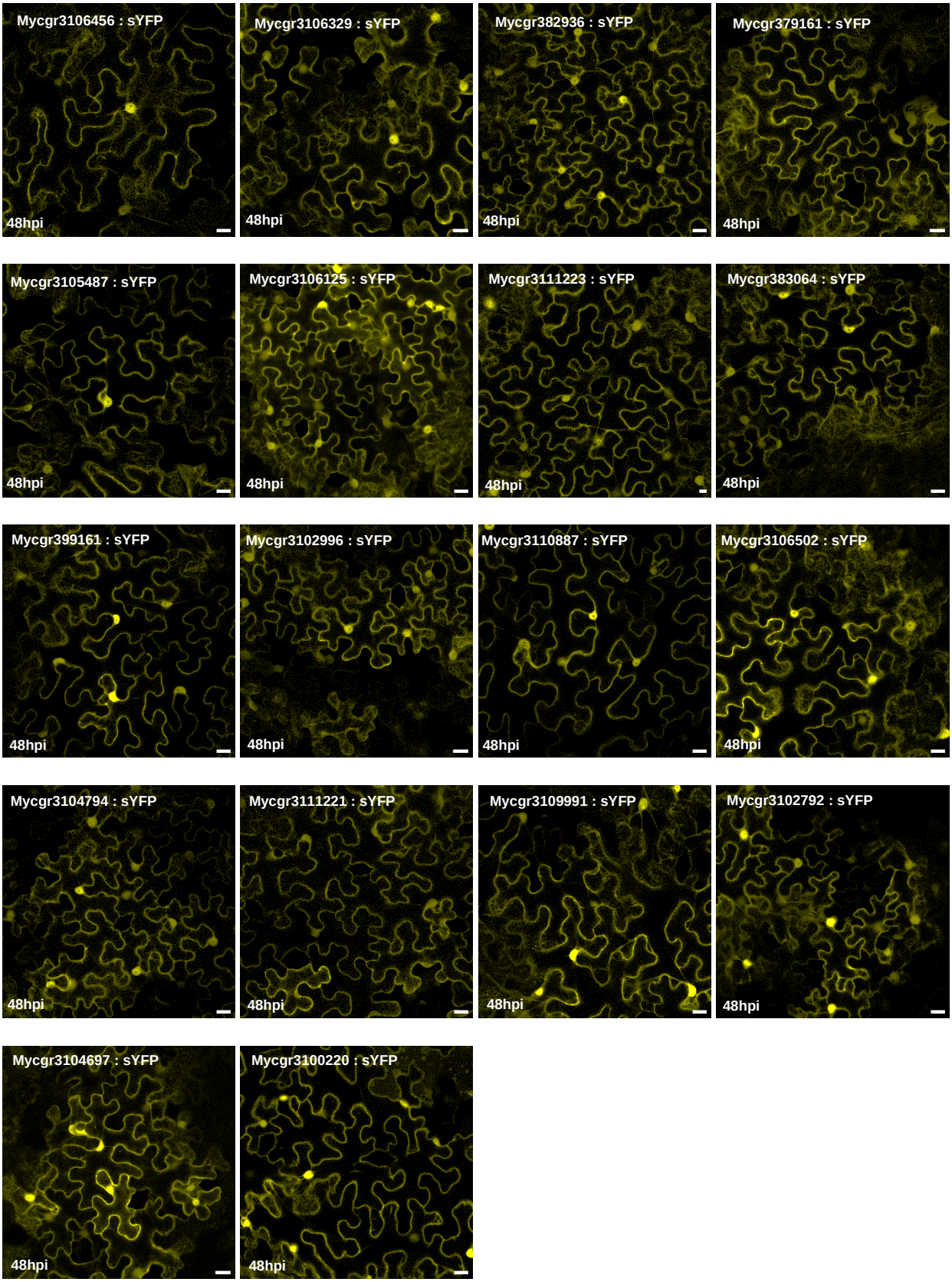
Mycgr3106456 : sYFP
48hpi
Mycgr3106329 : sYFP
48hpi
Mycgr382936 : sYFP
48hpi
Mycgr379161 : sYFP
48hpi
Mycgr3105487 : sYFP
48hpi
Mycgr3106125 : sYFP
48hpi
Mycgr3111223 : sYFP
48hpi
Mycgr383064 : sYFP
48hpi
Mycgr399161 : sYFP
48hpi
Mycgr3102996 : sYFP
48hpi
Mycgr3110887 : sYFP
48hpi
Mycgr3106502 : sYFP
48hpi
Mycgr3104794 : sYFP
48hpi
Mycgr3111221 : sYFP
48hpi
Mycgr3109991 : sYFP
48hpi
Mycgr3102792 : sYFP
48hpi
Mycgr3104697 : sYFP
48hpi
Mycgr3100220 : sYFP
48hpi

Fig.11.

Zymoseptoria tritici candidate effectors display nucleo-cytosol localization in *Nicotiana benthamiana*. sYFP-tagged *Z. tritici* candidate effectors were transiently expressed in *N. benthamiana* leaves using agroinfiltration. Confocal micrographs of leaf epidermal cells were captured 48 hours following agroinfiltration. The scale bars shown represent 20 µM. Free sYFP was included as a reference control for nucleo-cytosol localization. All confocal micrographs are of single optical sections.

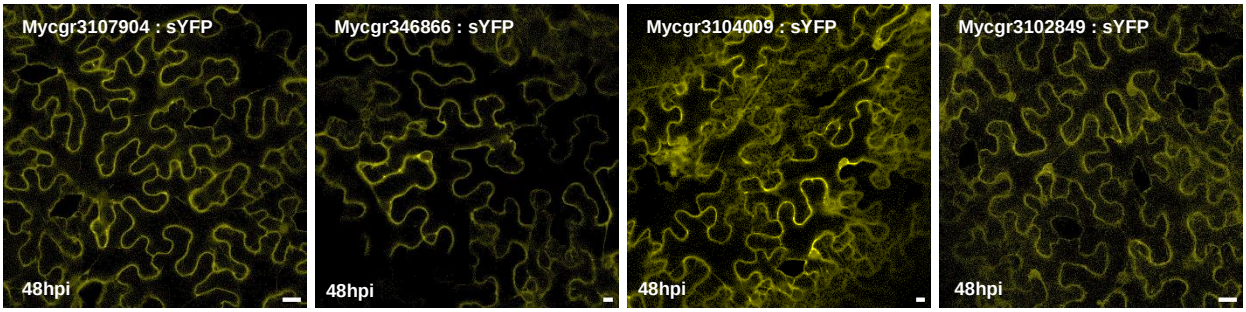

Fig. 12.

Four *Zymoseptoria tritici* candidate effectors localize predominantly to the cytosol. The indicated constructs were transiently expressed in *Nicotiana benthamiana* using agroinfiltration and live-cell imaging of epidermal cells was performed 48 hours following agroinfiltration. The scale bars shown represent 20 µM and all confocal micrographs are of single optical sections.

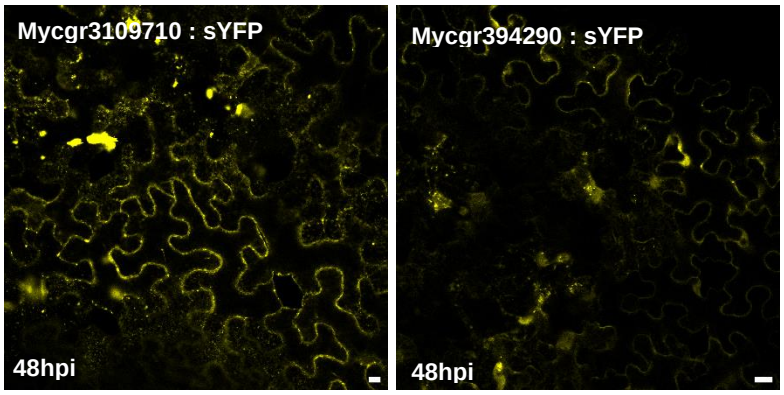

Fig. 13.

The Mycgr3109710- and Mycgr394290-fluorescent proteins accumulate in mobile cytosolic elements in *Nicotiana benthamiana* cells. The sYFP-tagged constructs were transiently expressed in *N. benthamiana* using agroinfiltration and live-cell imaging of epidermal cells was performed 48 hours following agroinfiltration. The scale bars shown represent 20 µM and all confocal micrographs are of single optical sections.

Supplementary Figures

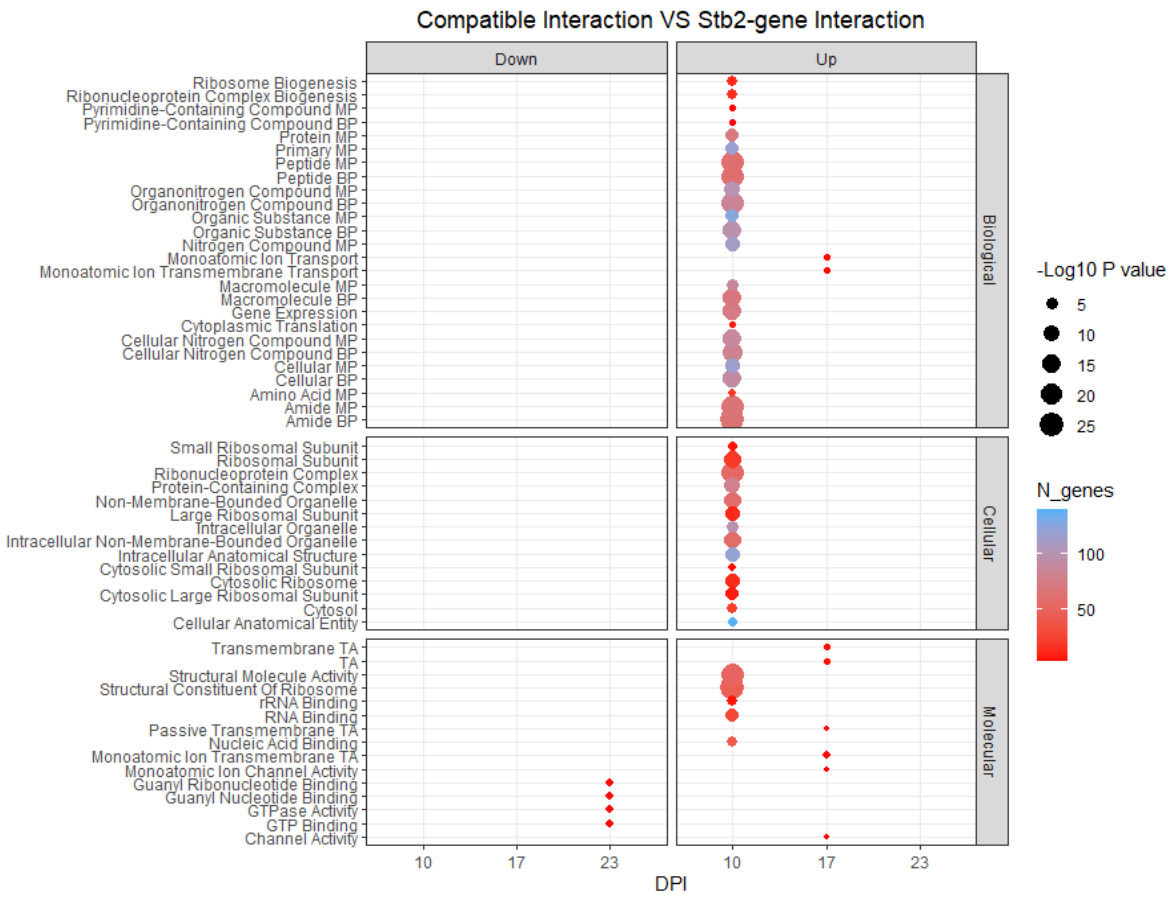

907

908 **Fig. S1.** Gene Ontology terms enriched at 10, 17 and 23 DPI in the compatible interaction

909 compared to the incompatible interaction on the Veranopolis cultivar. Metabolic process (MP),

910 Biosynthetic process (BP), Transporter Activity (TA). Organic compound (OC), Phosphatase

911 Activity (PA), Oxidoreductase activity (OA).

912

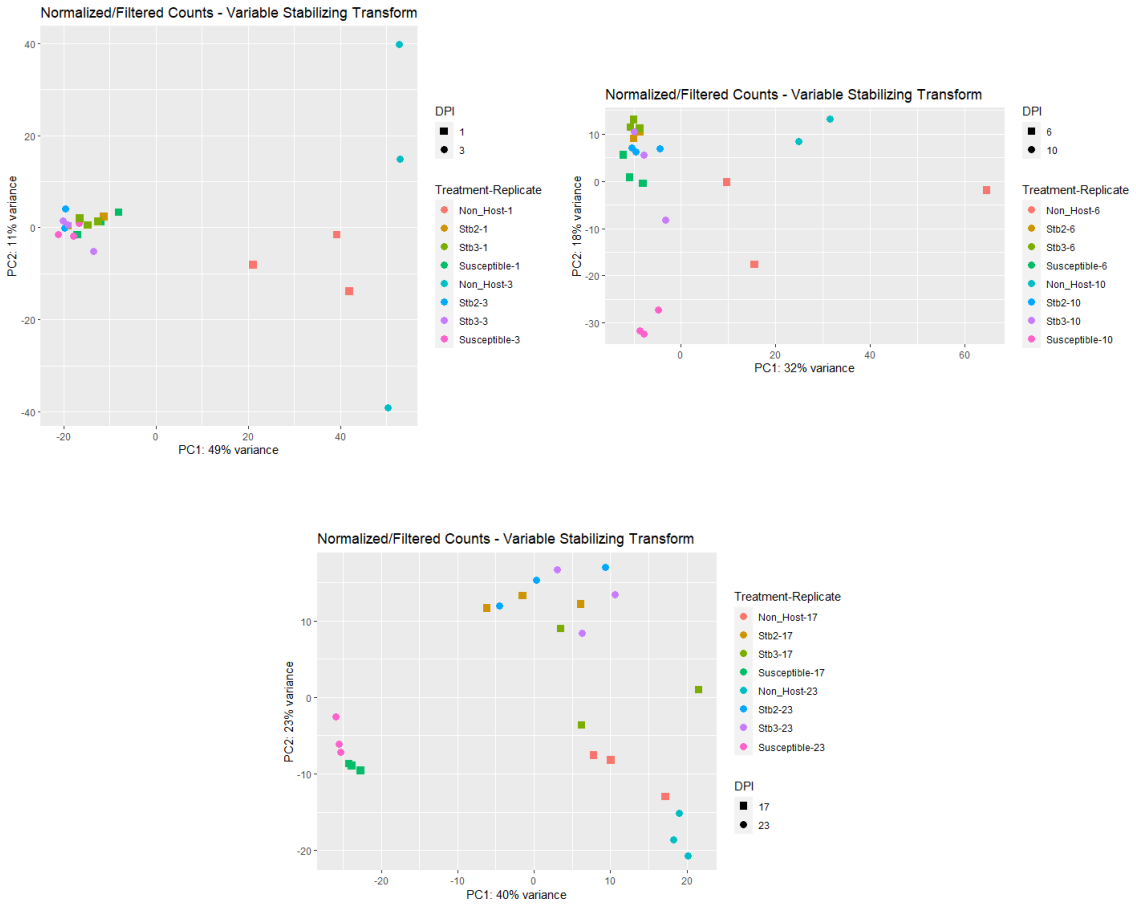

Fig. S2. Principal component analysis (PCA) of the normalized filtered read counts for RNA of *Zymoseptoria tritici* inoculated onto the highly susceptible wheat cultivar Taichung 29 (Susceptible) or the R-gene-containing resistant wheat cultivars Veranopolis (*Stb2*) or Israel 493 (*Stb3*) or the non-host barley at A) 1 and 3 B) 6 and 10 C) 17 and 23 days post inoculation (DPI).

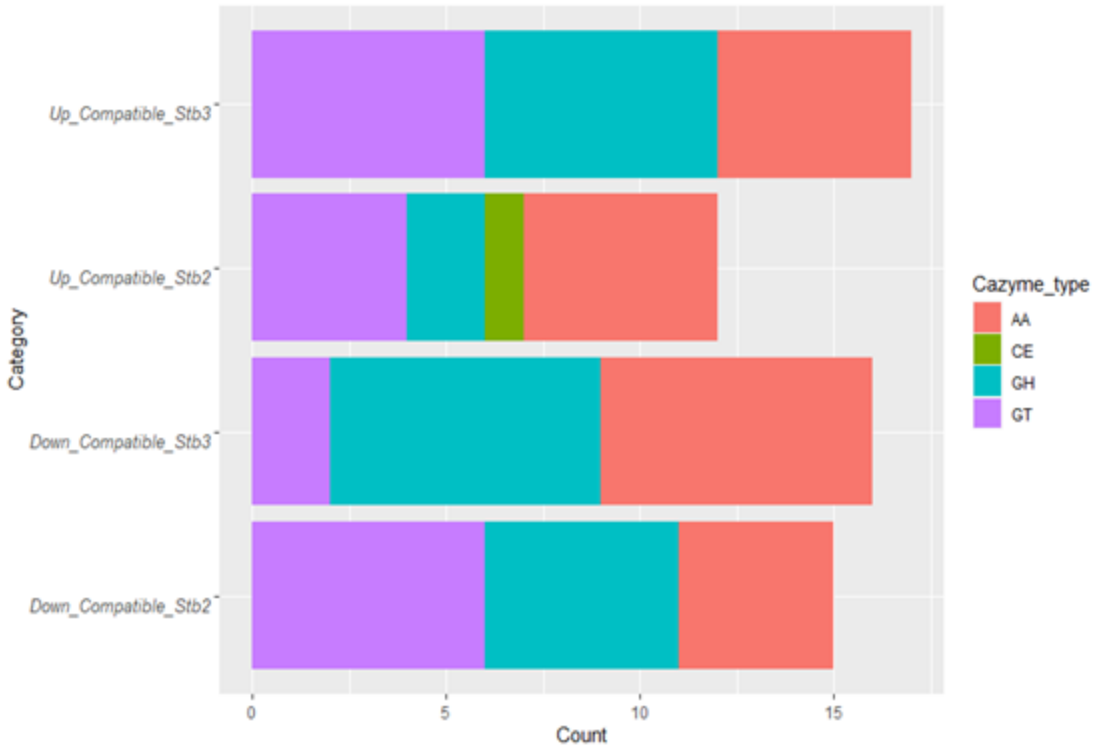

Fig. S3. Carbohydrate active enzymes of *Zymoseptoria tritici* identified at 1, 3, 6 and 10 DPI in the comparison between compatible and incompatible interactions.

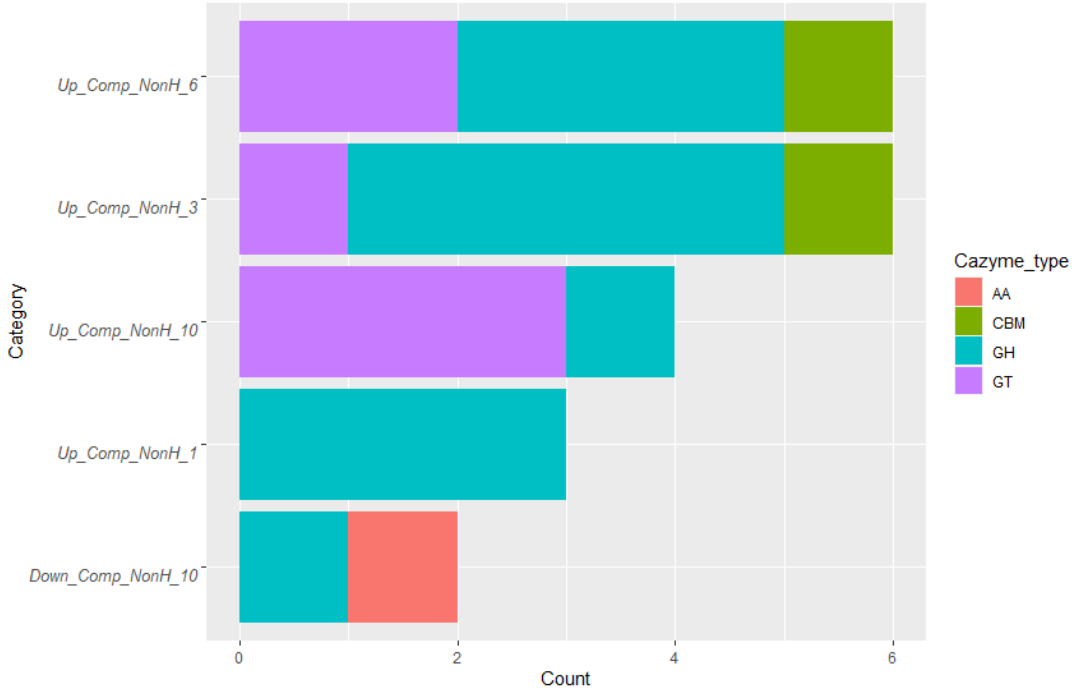

Fig. S4. Carbohydrate active enzymes of *Zymoseptoria tritici* identified at 1, 3, 6 and 10 DPI in the comparison between compatible and non-host interaction.

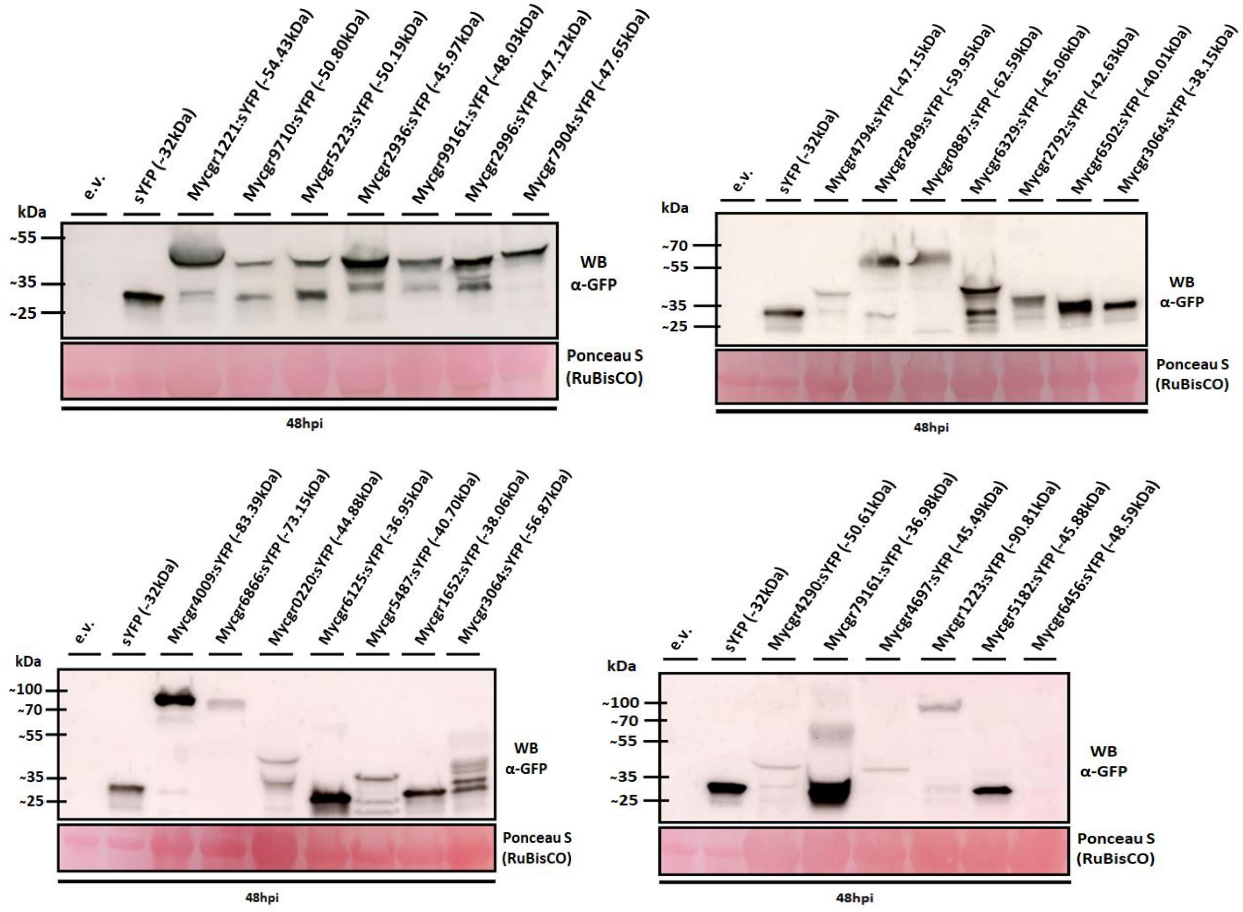

Fig. S5. Immunoblot analyses of the *Zymoseptoria tritici* effector-fluorescent protein fusions.

Literature Cited

Adhikari, T.B., Balaji, B., Breeden, J.D., and Goodwin, S.B. 2007. Resistance of wheat to *Mycosphaerella graminicola* involves early and late peaks of gene expression. Physiol. Mol. Plant Pathol. 71:55–68.

Amezrou, R., Audéon, C., Compain, J., Gélisse, S., Ducasse, A., Saintenac, C., Lapalu, N., Louet, C., Orford, S., Croll, D., Amselem, J., Fillinger, S., & Marcel, T. C. (2023). A secreted protease-like protein in *Zymoseptoria tritici* is responsible for avirulence on Stb9 resistance gene in wheat. *PLOS Pathogens*, *19*(5), e1011376. https://doi.org/10.1371/journal.ppat.1011376

Anders, S., Pyl, P. T., & Huber, W. (2015). HTSeq—A Python framework to work with high-throughput sequencing data. *Bioinformatics*, *31*(2), 166–169. https://doi.org/10.1093/bioinformatics/btu638

Ben, S., Barek, M., Cordewener, J. H. G., Tabib, S. M., Lee, T. A. J. V. D., Liu, Z., Mirzadi, A., Mehrabi, R., America, A. H. P., Robert, O., Friesen, T. L., Hamza, S., Stergiopoulos, I., Wit, P. J. G. M. D., & Kema, G. H. J. (2015). FPLC and liquid-chromatography mass spectrometry identify candidate necrosis-inducing proteins from culture filtrates of the fungal wheat pathogen *Zymoseptoria tritici*. *Fungal Genetics and Biology*, *79*, 54–62. https://doi.org/10.1016/j.fgb.2015.03.015

Brown, J. K. M., Chartrain, L., Lasserre-Zuber, P., & Saintenac, C. (2015). Genetics of resistance to *Zymoseptoria tritici* and applications to wheat breeding. *Fungal Genetics and Biology*, *79*, 33–41. https://doi.org/10.1016/j.fgb.2015.04.017

Bu, D., Luo, H., Huo, P., Wang, Z., Zhang, S., He, Z., Wu, Y., Zhao, L., Liu, J., Guo, J., Fang, S., Cao, W., Yi, L., Zhao, Y., & Kong, L. (2021). KOBAS-i: Intelligent prioritization and exploratory visualization of biological functions for gene enrichment analysis. *Nucleic Acids Research*, *49*(W1), W317–W325. https://doi.org/10.1093/nar/gkab447

Goodwin, S. B., M'Barek, S. B., Dhillon, B., Wittenberg, A. H. J., Crane, C. F., Hane, J. K., Foster, A. J., van der Lee, T. A. J., Grimwood, J., Aerts, A., Antoniw, J., Bailey, A., Bluhm, B., Bowler, J., Bristow, J., van der Burgt, A., Canto-Canché, B., Churchill, A. C. L., Conde-Ferràez, L., … Kema, G. H. J. (2011). Finished genome of the fungal wheat pathogen *Mycosphaerella graminicola* reveals dispensome structure, chromosome plasticity, and stealth pathogenesis. *PLoS Genetics*, *7*(6), 1002070. https://doi.org/10.1371/journal.pgen.1002070

Hallgren, J., Tsirigos, K. D., Pedersen, M. D., Armenteros, J. J. A., Marcatili, P., Nielsen, H., Krogh, A., & Winther, O. (2022). DeepTMHMM predicts alpha and beta transmembrane proteins using deep neural networks (p. 2022.04.08.487609). bioRxiv. https://doi.org/10.1101/2022.04.08.487609

Jelenska, J., Yao, N., Vinatzer, B. A., Wright, C. M., Brodsky, J. L., & Greenberg, J. T. (2007). A J-domain Virulence Effector of *Pseudomonas syringae* Remodels Host Chloroplasts and Suppresses Defenses. *Current Biology : CB*, *17*(6), 499–508. https://doi.org/10.1016/j.cub.2007.02.028

Käll, L., Krogh, A., & Sonnhammer, E. L. L. (2004). A Combined Transmembrane Topology and Signal Peptide Prediction Method. *Journal of Molecular Biology*, *338*(5), 1027–1036. https://doi.org/10.1016/j.jmb.2004.03.016

Kanehisa, M., Furumichi, M., Tanabe, M., Sato, Y., & Morishima, K. (2017). KEGG: New perspectives on genomes, pathways, diseases and drugs. *Nucleic Acids Research*, *45*(Database issue), D353–D361. https://doi.org/10.1093/nar/gkw1092

Karki, S. J., Reilly, A., Zhou, B., Mascarello, M., Burke, J., Doohan, F., Douchkov, D., & Schweizer, P. (2021). A small secreted protein from *Zymoseptoria tritici* interacts with a wheat E3 ubiquitin ligase to promote disease. *72*(2), 733–746. https://doi.org/10.1093/jxb/eraa489

Kellner, R., Bhattacharyya, A., Poppe, S., Hsu, T. Y., Brem, R. B., & Stukenbrock, E. H. (2014). Expression profiling of the wheat pathogen *Zymoseptoria tritici* reveals genomic patterns of transcription and host-specific regulatory programs. *Genome Biology and Evolution*, *6*(6), 1353–1365. https://doi.org/10.1093/gbe/evu101

Laugé, R., Joosten, M. H. A. J., Van den Ackerveken, G. F. J. M., Van den Broek, H. W. J., & De Wit, P. J. G. M. (1997). The In Planta-Produced Extracellular Proteins ECP1 and ECP2 of *Cladosporium fulvum* Are Virulence Factors. *Molecular Plant-Microbe Interactions*®, *10*(6), 725–734. https://doi.org/10.1094/MPMI.1997.10.6.725

Li, S., Dong, Y., Li, L., Zhang, Y., Yang, X., Zeng, H., Shi, M., Pei, X., Qiu, D., & Yuan, Q. (2019). The Novel Cerato-Platanin-Like Protein FocCP1 from *Fusarium oxysporum* Triggers an Immune Response in Plants. *International Journal of Molecular Sciences*, *20*(11), 2849. https://doi.org/10.3390/ijms20112849

Love, M. I., Huber, W., & Anders, S. (2014). Moderated estimation of fold change and dispersion for RNA-seq data with DESeq2. *Genome Biology*, *15*(12), 550. https://doi.org/10.1186/s13059-014-0550-8

Lu, S., & Edwards, M. C. (2018). Molecular Characterization and Functional Analysis of PR-1-Like Proteins Identified from the Wheat Head Blight Fungus *Fusarium graminearum*. *Phytopathology®*, *108*(4), 510–520. https://doi.org/10.1094/PHYTO-08-17-0268-R

Marshall, R., Kombrink, A., Motteram, J., Loza-reyes, E., Lucas, J., Hammond-kosack, K. E., Thomma, B. P. H. J., & Rudd, J. J. (2011). Analysis of Two in Planta Expressed LysM Effector Homologs from the Fungus *Mycosphaerella graminicola* Reveals Novel Functional Properties and Varying Contributions to Virulence on Wheat 1 [W][OA]. *156*(June), 756–769. https://doi.org/10.1104/pp.111.176347

Meshram, S., Gogoi, R., Bashyal, B. M., Kumar, A., Mandal, P. K., & Hossain, F. (2022). Comparative Transcriptome Analysis of Fungal Pathogen *Bipolaris maydis* to Understand Pathogenicity Behavior on Resistant and Susceptible Non-CMS Maize Genotypes. *Frontiers in Microbiology*, *13*, 837056. https://doi.org/10.3389/fmicb.2022.837056

Mirzadi Gohari, A., Ware, S. B., Wittenberg, A. H. J., Mehrabi, R., Ben M'Barek, S., Verstappen, E. C. P., van der Lee, T. A. J., Robert, O., Schouten, H. J., de Wit, P. P. J. G. M., & Kema, G. H. J. (2015). Effector discovery in the fungal wheat pathogen *Zymoseptoria tritici*. *Molecular Plant Pathology*, *16*(9), 931–945. https://doi.org/10.1111/mpp.12251

Palma-Guerrero, J., Ma, X., Torriani, S. F. F., Zala, M., Francisco, C. S., Hartmann, F. E., Croll, D., & McDonald, B. A. (2017). Comparative Transcriptome Analyses in *Zymoseptoria tritici* Reveal Significant Differences in Gene Expression Among Strains During Plant Infection. *Molecular Plant-Microbe Interactions®*, *30*(3), 231–244. https://doi.org/10.1094/MPMI-07-16-0146-R

Pečenková, T., Pejchar, P., Moravec, T., Drs, M., Haluška, S., Šantrůček, J., Potocká, A., Žárský, V., & Potocký, M. (2022). Immunity functions of *Arabidopsis* pathogenesis-related 1 are coupled but not confined to its C-terminus processing and trafficking. *Molecular Plant Pathology*, *23*(5), 664–678. https://doi.org/10.1111/mpp.13187

Quarantin, A., Castiglioni, C., Schäfer, W., Favaron, F., & Sella, L. (2019). The *Fusarium graminearum* cerato-platanins loosen cellulose substrates enhancing fungal cellulase activity as expansin-like proteins. *Plant Physiology and Biochemistry*, *139*, 229–238. https://doi.org/10.1016/j.plaphy.2019.03.025

Raudvere, U., Kolberg, L., Kuzmin, I., Arak, T., Adler, P., Peterson, H., & Vilo, J. (2019). g:Profiler: A web server for functional enrichment analysis and conversions of gene lists (2019 update). *Nucleic Acids Research*, *47*(W1), W191–W198. https://doi.org/10.1093/nar/gkz369

Rocafort, M., Fudal, I., & Mesarich, C. H. (2020). Apoplastic effector proteins of plant-associated fungi and oomycetes. *Current Opinion in Plant Biology*, *56*, 9–19. https://doi.org/10.1016/j.pbi.2020.02.004

Rudd, J. J., Kanyuka, K., Hassani-Pak, K., Derbyshire, M., Andongabo, A., Devonshire, J., Lysenko, A., Saqi, M., Desai, N. M., Powers, S. J., Hooper, J., Ambroso, L., Bharti, A., Farmer, A., Hammond-Kosack, K. E., Dietrich, R. A., & Courbot, M. (2015). Transcriptome and metabolite profiling of the infection cycle of *Zymoseptoria tritici* on wheat reveals a biphasic interaction with plant immunity involving differential pathogen chromosomal contributions and a variation on the hemibiotrophic lifestyle definition. *Plant Physiology*, *167*(3), 1158–1185. https://doi.org/10.1104/pp.114.255927

Saintenac, C., Cambon, F., Aouini, L., Verstappen, E., Ghaffary, S. M. T., Poucet, T., Marande, W., Berges, H., Xu, S., Jaouannet, M., Favery, B., Alassimone, J., Sánchez-Vallet, A., Faris, J., Kema, G., Robert, O., & Langin, T. (2021). A wheat cysteine-rich receptor-like kinase confers broad-spectrum resistance against Septoria tritici blotch. *Nature Communications*, *12*, 433. https://doi.org/10.1038/s41467-020-20685-0

Saintenac, C., Lee, W.-S., Cambon, F., Rudd, J. J., King, R. C., Marande, W., Powers, S. J., Bergès, H., Phillips, A. L., Uauy, C., Hammond-Kosack, K. E., Langin, T., & Kanyuka, K. (2018). Wheat receptor-kinase-like protein Stb6 controls gene-for-gene resistance to fungal pathogen *Zymoseptoria tritici*. *Nature Genetics*, *50*(3), Article 3. https://doi.org/10.1038/s41588-018-0051-x

Sánchez-Vallet, A., Saleem-Batcha, R., Kombrink, A., Hansen, G., Valkenburg, D.-J., Thomma, B. P., & Mesters, J. R. (2013). Fungal effector Ecp6 outcompetes host immune receptor

for chitin binding through intrachain LysM dimerization. *ELife*, *2*, e00790. https://doi.org/10.7554/eLife.00790

Sánchez-Vallet, A., Tian, H., Rodriguez-Moreno, L., Valkenburg, D.-J., Saleem-Batcha, R., Wawra, S., Kombrink, A., Verhage, L., de Jonge, R., van Esse, H. P., Zuccaro, A., Croll, D., Mesters, J. R., & Thomma, B. P. H. J. (2020). A secreted LysM effector protects fungal hyphae through chitin-dependent homodimer polymerization. *PLoS Pathogens*, *16*(6), e1008652. https://doi.org/10.1371/journal.ppat.1008652

Sperschneider, J., Catanzariti, A.-M., DeBoer, K., Petre, B., Gardiner, D. M., Singh, K. B., Dodds, P. N., & Taylor, J. M. (2017). LOCALIZER: Subcellular localization prediction of both plant and effector proteins in the plant cell. *Scientific Reports*, *7*(1), Article 1. https://doi.org/10.1038/srep44598

Sperschneider, J., & Dodds, P. N. (2022). EffectorP 3.0: Prediction of Apoplastic and Cytoplasmic Effectors in Fungi and Oomycetes. *Molecular Plant-Microbe Interactions®*, *35*(2), 146–156. https://doi.org/10.1094/MPMI-08-21-0201-R

Sperschneider, J., Dodds, P. N., Singh, K. B., & Taylor, J. M. (2018). ApoplastP: Prediction of effectors and plant proteins in the apoplast using machine learning. *New Phytologist*, *217*(4), 1764–1778. https://doi.org/10.1111/nph.14946

Stergiopoulos, I., Burg, H. A. V. D., Ökmen, B., Beenen, H. G., Liere, S. V., & Kema, G. H. J. (2010). Tomato *Cf* resistance proteins mediate recognition of cognate homologous effectors from fungi pathogenic on dicots and monocots. https://doi.org/10.1073/pnas.1002910107

Stergiopoulos, I., Kourmpetis, Y. A. I., Slot, J. C., Bakker, F. T., Wit, P. J. G. M. D., & Rokas, A. (2012). In Silico Characterization and Molecular Evolutionary Analysis of a Novel Superfamily of Fungal Effector Proteins. *29*(11), 3371–3384. https://doi.org/10.1093/molbev/mss143

Teixeira, P. J. P. L., Thomazella, D. P. T., Vidal, R. O., Prado, P. F. V. do, Reis, O., Baroni, R. M., Franco, S. F., Mieczkowski, P., Pereira, G. A. G., & Mondego, J. M. C. (2012). The Fungal Pathogen *Moniliophthora perniciosa* Has Genes Similar to Plant PR-1 That Are Highly Expressed during Its Interaction with Cacao. *PLOS ONE*, *7*(9), e45929. https://doi.org/10.1371/journal.pone.0045929

Teufel, F., Almagro Armenteros, J. J., Johansen, A. R., Gíslason, M. H., Pihl, S. I., Tsirigos, K. D., Winther, O., Brunak, S., von Heijne, G., & Nielsen, H. (2022). SignalP 6.0 predicts all five types of signal peptides using protein language models. *Nature Biotechnology*, *40*(7), 1023–1025. https://doi.org/10.1038/s41587-021-01156-3

Tian, H., MacKenzie, C. I., Rodriguez-Moreno, L., van den Berg, G. C. M., Chen, H., Rudd, J. J., Mesters, J. R., & Thomma, B. P. H. J. (2021). Three LysM effectors of *Zymoseptoria tritici* collectively disarm chitin-triggered plant immunity. *Molecular Plant Pathology*, *22*(6), 683–693. https://doi.org/10.1111/mpp.13055

Tintor, N., Nieuweboer, G. A. M., Bakker, I. A. W., & Takken, F. L. W. (2022). The Intracellularly Acting Effector Foa3 Suppresses Defense Responses When Infiltrated Into the Apoplast. *Frontiers in Plant Science*, *13*, 813181. https://doi.org/10.3389/fpls.2022.813181

Wangorsch, A., Scheurer, S., Blanca, M., Blanca-Lopez, N., Somoza, M. L., & Martín-Pedraza, L. (2022). Allergenic Properties and Molecular Characteristics of PR-1 Proteins. *Frontiers in Allergy*, *3*, 824717. https://doi.org/10.3389/falgy.2022.824717

Yang, F., Li, W., & Jørgensen, H. J. L. (2013). Transcriptional reprogramming of wheat and the hemibiotrophic pathogen *Septoria tritici* during two phases of the compatible interaction. *PLoS ONE*, *8*(11), 1–15. https://doi.org/10.1371/journal.pone.0081606

Yang, G., Tang, L., Gong, Y., Xie, J., Fu, Y., Jiang, D., Li, G., Collinge, D. B., Chen, W., & Cheng, J. (2018). A cerato-platanin protein SsCP1 targets plant PR1 and contributes to virulence of *Sclerotinia sclerotiorum*. *New Phytologist*, *217*(2), 739–755. https://doi.org/10.1111/nph.14842

Zhang, M., Xie, S., Zhao, L., Meng, X., Song, L., Feng, H., & Huang, L. (2019). Hce2 domain-containing effectors contribute to the full virulence of *Valsa mali* in a redundant manner. *0*, 843–856. https://doi.org/10.1111/mpp.12796

Zhong, Z., Marcel, T. C., Hartmann, F. E., Ma, X., Plissonneau, C., Zala, M., Ducasse, A., Confais, J., Compain, J., Lapalu, N., Amselem, J., McDonald, B. A., Croll, D., & Palma-Guerrero, J. (2017). A small secreted protein in *Zymoseptoria tritici* is responsible for avirulence on wheat cultivars carrying the Stb6 resistance gene. *New Phytologist*, *214*(2), 619–631. https://doi.org/10.1111/nph.14434